RSC Advances

PAPER

View Article Online
View Journal | View Issue

Cite this: *RSC Adv.*, 2025, **15**, 42698

First-principles insights into thermo-mechanical, electronic, and optical properties of Hf_2AC (A = Cl, Br) MAX phases through A-site halogen tuning

Asif Mohammed Arfi,[ae] Mahamudun Nabi,[b] Md. Hasan Mia,*[c] Omar Alsalmi,[d] Muhammad Athar Uddin[e] and Md. Zahid Hasan *[f]

In this study, we conduct a comprehensive first-principles investigation of the mechanical, electronic, optical, and thermo-mechanical properties of Hf_2AC MAX phases, where the A-site halogen is varied between Cl and Br. We use density functional theory to look into how changing the A-site atom affects the structural stability and other functional properties of these layered ternary carbides. Structural analysis reveals that replacing Cl with the larger Br atom increases lattice constants and unit cell volume, aligning with the atomic size trend. Both phases satisfy key stability criteria, including thermodynamic, mechanical, and dynamic stability, confirmed by formation energies, elastic constants, and phonon dispersions. Mechanical property analysis shows that Hf_2BrC has slightly reduced stiffness compared to Hf_2ClC due to weaker Hf–Br bonding, though both maintain ductility and mechanical robustness. Thermo-mechanical parameters, such as Debye temperature, melting point, and thermal conductivity, are influenced by halogen mass and bonding character. Thermo-lattice properties, including heat capacity and the Grüneisen parameter, further support their thermal stability over a broad temperature range. The electronic band structures and density of states show that both compounds act like metals, with Hf d-orbitals at the Fermi level being the most important. Optical properties, derived from the dielectric function, indicate strong activity in the visible and ultraviolet regions. Br substitution causes a red shift in absorption and reflectivity spectra, enhancing plasmonic and photonic behavior. High reflectivity and photoconductivity beyond the plasma frequency highlight their potential in optoelectronic and UV shielding applications. The ability to fine-tune these materials through atomic-level modifications opens new pathways for designing MAX phases with tailored performance for use in coatings, electronics, and energy-related applications.

Received 25th September 2025
Accepted 27th October 2025

DOI: 10.1039/d5ra07272g

rsc.li/rsc-advances

1. Introduction

MAX phases, a unique class of layered ternary carbides and nitrides, have garnered significant scientific interest owing to their remarkable combination of metallic and ceramic characteristics. These materials are structurally resilient at high temperatures, exhibit excellent machinability, and demonstrate superior electrical and thermal conductivity along with exceptional resistance to thermal shock, corrosion, and oxidation.[1–3] Such a blend of properties makes MAX phases ideal for a wide array of high-performance industrial applications, including machinable refractories, heating elements, rotating electrical contacts, bearings, nozzles, die-pressing tools, and heat exchangers. Notably, their ability to withstand neutron irradiation has also led to investigations into their potential roles in nuclear reactor components.[4] In recent years, several MAX phases have also been explored as potential candidates for thermal barrier coatings (TBCs), given their favorable thermal and mechanical behavior at elevated temperatures.[5,6]

Structurally, MAX phases are characterized by a hexagonal layered lattice and are described by the general chemical formula $M_{n+1}AX_n$, where M is an early transition metal, A is an element from groups 13 to 17 of the periodic table, and X is either carbon or nitrogen.[2] The integer n indicates the number of M–X layers in the structure; for $n = 1$, the resulting formula becomes M_2AX, known as the 211-type MAX phase, which is the focus of this investigation.[2,5,7]

[a]*Dept of Computer Science and Engineering, University of Yamanashi, Takeda, 4-4-37 Kofu, Yamanashi, Japan*

[b]*Department of Physics, University of Rajshahi, Rajshahi 6205, Bangladesh*

[c]*Department of Computer and Communication Engineering, International Islamic University Chittagong Kumira, Chattogram, 4318, Bangladesh. E-mail: mdhasan111.ru@gmail.com*

[d]*Department of Physics, College of Science, Umm Al-Qura University, Makkah 21955, Saudi Arabia*

[e]*Department of Electrical and Electronic Engineering, International Islamic University Chittagong, Kumira, Chittagong, 4318, Bangladesh*

[f]*Materials Research and Simulation Lab, Department of Electrical and Electronic Engineering, International Islamic University Chittagong, Kumira, Chittagong, 4318, Bangladesh. E-mail: zahidhasan.02@gmail.com*

Over 60 stable ternary MAX phases have been experimentally synthesized, and numerous solid solutions have been reported through substitution at the M and A sites. Common examples include (Nb, Zr)$_2$AlC, (Ti, V)$_2$SC, (Ti, Hf)$_2$SC, V$_2$(Al, Ga)C, Ti$_2$(Si, Ge)C, and Cr$_2$(Al, Ge)C.[8–15] However, A-site solid solutions are typically limited to elements from groups 13 to 16, such as Al, Si, or Ga. Recently, a new class of MAX phases has emerged where halogen elements (Cl, Br, I) replace the conventional A-site elements. These include compounds such as La$_2$Br(C, N), La$_2$Cl(C, N), Sc$_2$ClC, Sc$_2$BrC, Hf$_2$ClC, and Hf$_2$BrC, which indicate the structural feasibility of incorporating halogens at the A site in MAX-like frameworks.[2]

The unique characteristics of M$_2$AX phases, commonly referred to as "211" MAX phases, have captivated the scientific community due to their remarkable combination of metallic and ceramic properties. These materials exhibit a fascinating array of attributes: moderate hardness (Vickers hardness of 2.0–8.0 GPa), anisotropy, elastic stiffness, excellent machinability, damage tolerance, and high-temperature plasticity.[16] They are lightweight, resistant to fatigue, creep, oxidation, and thermal shock, and demonstrate a transition from brittleness to plasticity at elevated temperatures. These extraordinary features make MAX phases highly desirable for diverse technological applications. Recent studies have further expanded the understanding of M$_2$AX phases, showcasing their multifunctionality. For instance, H. Kim *et al.*[17] identified M$_2$AX phases (M = lanthanides, A = Al or Si, X = C or N) as exceptional candidates for bond coat applications. Similarly, O. S. Rijal *et al.*[18] explored the properties of Ti$_2$CdC and Ti$_2$SC, revealing their potential in optoelectronics, advanced photonic devices, solar thermal collectors, and thermal insulation. The works of B. U. Haq *et al.*[19] and M. N. Amin *et al.*[20] have highlighted the applications of W$_2$GaX and Cr$_2$AC phases, respectively, in high-temperature environments, optoelectronic devices, and other advanced technologies. Furthermore, W. Tan *et al.*[21] demonstrated the potential of S-based M$_2$SX phases in thermoelectric applications, while M. A. Ali *et al.*[22] and M. M. Uddin *et al.*[23] underscored the suitability of Hf$_2$SeC, Hf$_2$AlC, and Hf$_2$AlN for high-temperature and solar heating reduction applications.

Despite these advances, a comprehensive understanding of how halogen substitution at the A site influences the physical properties of MAX phases is still lacking.

The prior work by Ohmer *et al.*[2] focused on predicting the elastic constants and moduli of Hf$_2$ClC and Hf$_2$BrC within a broad high-throughput screening of 82 potential MAX phases, using basic thermodynamic descriptors to assess phase stability. While this study was foundational in identifying the existence of these compounds, it primarily addressed phase feasibility rather than functional behavior. In contrast, our present study provides a comprehensive, in-depth, and comparative investigation of the functional properties influenced by halogen substitution in Hf-based MAX phases, extending well beyond prior structural predictions and providing helpful information regarding their mechanical, electronic, thermal, and optical behavior. We systematically explore their thermo-mechanical responses by analyzing elastic anisotropy indices, Debye and melting temperatures, the Grüneisen parameter, and both lattice and minimum thermal conductivities, which are critical for understanding their thermal resilience and structural integrity. Additionally, we discuss their electronic structure through detailed assessments of band dispersion, directional charge carrier mobility, effective mass, and the nature of orbital hybridization—key insights necessary for electronic and energy-related applications. Furthermore, we present a complete evaluation of the optical behavior of these materials, including their dielectric functions, absorption characteristics, photoconductivity, reflectivity, and energy-loss spectra, which have not been previously reported. To the best of our knowledge, no earlier study has comprehensively examined the collective influence of halogen substitution (Cl *versus* Br) on such an extensive range of physical properties in Hf-based MAX phases. Our findings address this critical gap and present a valuable framework for the property-driven design of advanced MAX materials, highlighting their potential across multifunctional domains such as thermal barrier coatings, optoelectronics, and structural applications operating under extreme environments.

The arrangement of this paper is as follows: Section 2 describes the DFT computational setting. Section 3 presents and analyzes observations and their physical implications. Section 4 provides a brief summary of the present findings and concluding remarks.

2. DFT computational setting

In this work, we explore the impact of halogen substitution, specifically Cl and Br, at the A site of Hf$_2$AC (A = Cl, Br) MAX phases through comprehensive first-principles calculations based on density functional theory (DFT).[24] All calculations were performed using the CASTEP code,[25] a plane-wave-based density functional theory (DFT) software package. Ultrasoft pseudopotentials were employed for all atomic species (Hf, Cl, Br, and C), allowing accurate treatment of valence electron interactions while maintaining computational efficiency. To accurately capture the exchange–correlation interactions, we employed the generalized gradient approximation (GGA) using the Perdew–Burke–Ernzerhof (PBE) functional.[26] A plane-wave energy cutoff of 500 eV was selected to ensure convergence of total energy across all investigated systems. For Brillouin zone integration, a Monkhorst–Pack *k*-point mesh of 9 × 9 × 2 was used, offering an optimal balance between computational efficiency and numerical accuracy.[27] The interactions between valence electrons and ionic cores were described using ultrasoft pseudopotentials, which were carefully chosen to ensure reliable modeling of chemical bonding.[28] The valence states considered in our calculations were Hf ($5d^2 5s^2$), Cl ($3s^2 3p^5$), Br ($4s^2 4p^5$), and C ($2s^2 2p^2$), which play a critical role in defining the material properties of the Hf$_2$ClC and Hf$_2$BrC compounds. Geometry optimizations were carried out using the Broyden–Fletcher–Goldfarb–Shanno (BFGS) minimization algorithm.[29] The convergence thresholds were rigorously set to a total energy difference of 5×10^{-6} eV per atom, a maximum force of 0.01 eV Å^{-1}, a maximum stress of 0.02 GPa, and a maximum displacement of 5×10^{-4} Å. These strict criteria ensured that the

optimized structures were robust and well-suited for subsequent property evaluations. Following structural optimization, we systematically computed various mechanical properties of Hf_2ClC and Hf_2BrC, including their elastic constants *via* the stress–strain method.[30] Phonon dynamic properties, including the phonon dispersion and phonon density of states (PDOS), were calculated using the finite displacement method.[31] The crystallographic structures were visualized using the VESTA software package, providing insights into the atomic arrangements and symmetry.[32]

3. Observations and physical implications

3.1 Crystallographic properties

The substitution of halogen (Cl, Br) in Hf_2AC (A = Cl, Br) MAX phases induce significant changes in both the structural characteristics and properties of these compounds due to differences in atomic size, electronegativity, and bonding behavior. As illustrated in Fig. 1, these compounds crystallize in the hexagonal crystal system with the space group $P6_3/mmc$ (no. 194), with each unit cell containing eight atoms and two formula units. The atomic positions for Hf_2AC (A = Cl, Br) are defined by the Wyckoff coordinates: C atoms occupy the 2a site at (0, 0, 0), A-site atoms (Cl or Br) are located at 2c (1/3, 2/3, 1/4), and Hf atoms are positioned at 4f (2/3, 1/3, Z_M). The crystal structure is determined by two main lattice parameters, a and c, along with the internal atomic coordinate Z_M.

The primary effect of substituting Cl and Br in the A-site on Hf_2AC MAX phases is observed in the c/a ratio and unit cell volume. Hf_2BrC exhibits a slightly higher c/a ratio and unit cell volume than Hf_2ClC, which is consistent with the larger atomic radius of Br compared to Cl. The trend of increasing c/a ratio and unit cell volume with larger atoms is further confirmed by comparing Hf_2ClC and Hf_2BrC with other Hf-based MAX phases in Table 1. These changes in the crystal structure reflect a typical trend observed in MAX phases, where the incorporation of larger atoms leads to expanded interlayer spacing and a corresponding increase in unit cell volume. The equilibrium crystal structures of Hf_2AC (A = Cl, Br) have been optimized by minimizing the total energy, with the resulting structural parameters provided in Table 1. Although direct experimental or theoretical benchmarks for Hf_2ClC and Hf_2BrC are currently unavailable, our optimized values show strong consistency with those reported for other well-known and experimentally verified MAX phases, thereby reinforcing the reliability of our calculations and their alignment with established trends in the field (see Table 1).

3.2 Compound's stability

Since Hf_2AC (A = Cl, Br) are newly identified compounds with unexplored properties that have not yet been experimentally synthesized, our objective is to establish their theoretical foundation through density functional theory (DFT) calculations. This theoretical investigation aims to guide future experimental and computational studies. While we have

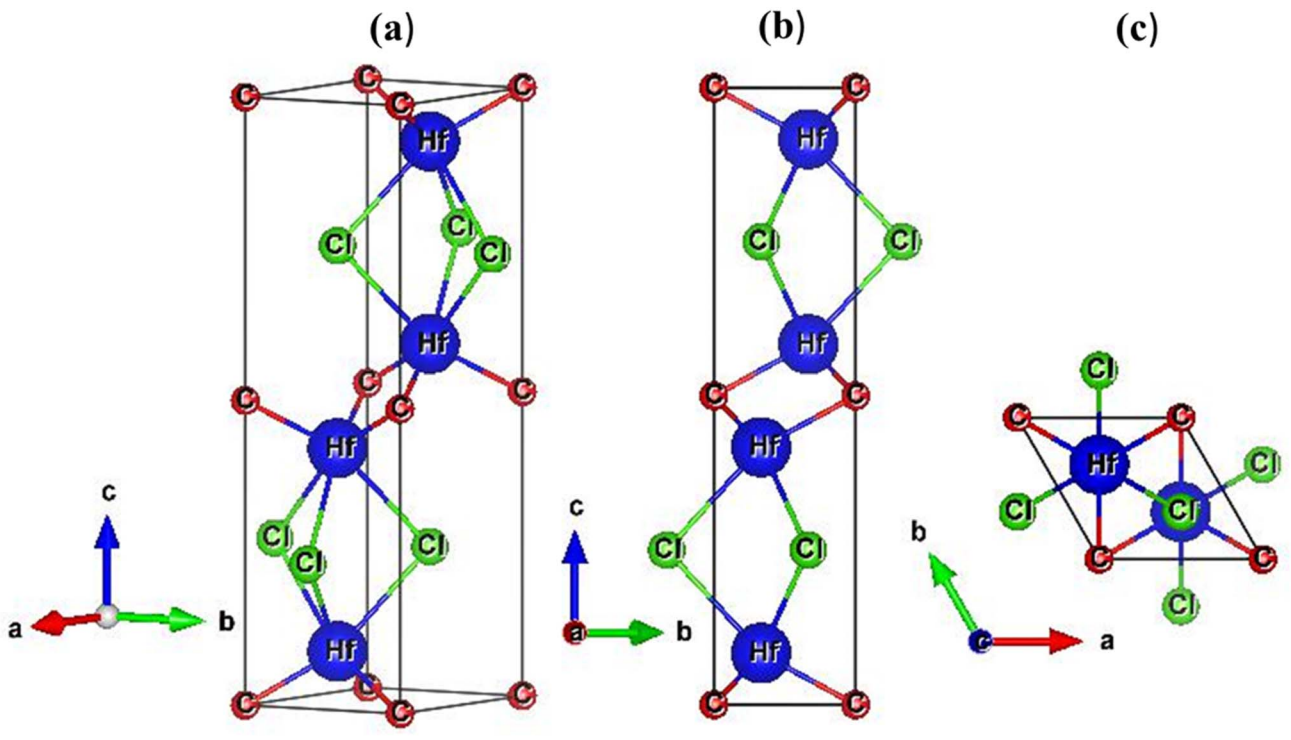

Fig. 1 Optimized crystal structures of Hf_2AC (A = Cl, Br) MAX phases: (a) standard orientation highlighting the layered hexagonal architecture, (b) projection along the a-axis emphasizing the stacking sequence, and (c) projection along the c-axis revealing the atomic arrangement within the basal plane.

Table 1 Structural and energetic properties of Hf_2AC (A = Cl, Br) MAX phases, featuring optimized lattice parameters (*a*, *c* in Å), *c*/*a* ratio, internal lattice parameter (Z_M in Å), unit cell volume (*V* in Å^3), formation enthalpy (ΔH_f in eV), formation energy (ΔE_f in eV) and coordination sites (O_r, P_r) along with theoretical comparisons

Phases	*a*	*c*	*c*/*a*	Z_M	*V*	ΔH_f	ΔE_f	O_r	P_r	Ref.
Hf_2ClC	3.432	12.947	3.77	0.0834	132.094	−7.13	−1.26	1.77	1.17	This
Hf_2BrC	3.490	13.427	3.84	0.0833	141.636	−6.95	−1.10	1.75	1.16	This
Hf_2AlC	3.275	14.362	4.39	0.0876						Expt.[36]
Hf_2SeB	3.522	12.478	3.54							Expt.[37]
Hf_2AlC	3.310	14.350	4.33	0.0890	136.345	—		—	—	Theo.[23]
Hf_2SC	3.423	12.196	3.56	0.1004	123.770	−8.16		—	—	Theo.[34]
Hf_2SnC	3.330	14.370	4.32	0.0879	138.006	—		—	—	Theo.[35]
Hf_2TlC	3.370	14.847	4.41	0.0825	146.025	—		—	—	Theo.[33]

predicted the stability of Hf_2ClC and Hf_2BrC using first-principles calculations, additional theoretical analyses may be necessary. Therefore, we conduct a comprehensive stability assessment of the Hf_2AC (A = Cl, Br) phases to provide insights for future experimental validation.

To evaluate the structural stability of Hf_2AC (A = Cl, Br), we examined the *c*/*a* ratio. For M_2AX-type phases, the ideal *c*/*a* value is approximately 4.89 (or $2\sqrt{6}$).[7,38] As shown in Table 1, the computed *c*/*a* values for Hf_2ClC (3.77) and Hf_2BrC (3.84) are reasonably close to this ideal value, indicating favorable structural stability.

Furthermore, in MAX phases, the spacing between the M and X (X = C, N) layers is characterized by the internal structural parameter z_m, which ideally takes a value of approximately 0.083 (or 1/12).[7,38] Our calculations reveal that the z_m values for Hf_2ClC and Hf_2BrC are close to this ideal value, indicating minimal deviation and further supporting structural stability (see Table 1).

To further assess stability, we analyzed distortions in the unit cell using the octahedral site (O_r) and trigonal prism site (P_r) parameters, defined as:[5]

$$O_r = \frac{\sqrt{3}}{2\sqrt{4{z_m}^2\left(\frac{c}{a}\right)^2 + \frac{1}{12}}} \text{ and } P_r = \frac{1}{\sqrt{\frac{1}{3} + \left(\frac{1}{4} - z_m\right)^2\left(\frac{c}{a}\right)^2}} \quad (1)$$

Ideally, both O_r and P_r should be equal to 1, with values greater or less than 1, indicating structural distortions. The O_r and P_r values for Hf_2ClC and Hf_2BrC are quite similar, with only slight differences. The slightly higher O_r and P_r values for Hf_2ClC compared to Hf_2BrC can be attributed to variations in atomic size, bonding characteristics, and structural distortions introduced by the halogen element (Cl *vs.* Br). Since Cl has a smaller atomic radius than Br, the interatomic spacing in the Hf_2ClC structure is slightly reduced compared to Hf_2BrC, leading to greater structural distortion. In contrast, the larger Br atoms in Hf_2BrC result in a more relaxed lattice structure with slightly reduced distortions, leading to lower O_r and P_r values. However, since these differences are small, both compounds remain structurally stable.

To evaluate their thermodynamic stability, we calculated the formation enthalpy (ΔH_f) and binding energy (ΔE_b), both of which serve as key indicators of stability. The formation enthalpy was computed using the following equations:[39]

$$\Delta H_f = \frac{E_{tot}(\text{Phase}) - lE_{Hf} - mE_A - nE_C}{N} < 0 \quad (2)$$

where, E_{tot}(Phase) represents the total energy of the Hf_2AC (A = Cl, Br) phase, while E_{Hf}, E_A, and E_C denote the atomic energies of Hf, A (Cl or Br), and C, respectively. The variables *l*, *m*, and *n* represent the number of atoms in the compound's empirical formula, while *N* indicates the total number of atoms in the formula unit. The calculated values of ΔH_f presented in Table 1, confirm the thermodynamic stability of both Hf_2ClC and Hf_2BrC. Moreover, similar negative energy values have been reported for other MAX phases.[4,5,7,40–42] This consistency suggests that Hf_2AC (A = Cl, Br) phase in our study is not only energetically favorable and exothermic but also highly stable.

Although the formation enthalpy (ΔH_f) provide insights into thermodynamic stability, it does not fully capture the stability of a compound. It is also essential to examine phase stability with respect to competing phases. This approach is particularly important in materials science, chemistry, and engineering, where real-world applications depend on the compound's resistance to decomposition into other stable phases. To address this, we analyzed the phase stability by comparing the total energies of Hf_2ClC and Hf_2BrC with those of relevant competing phases, as obtained from the Open Quantum Materials Database (OQMD).[43] For both compounds, the same set of competing phases was considered, although their compositional contributions differ slightly as dictated by the overall stoichiometry. The decomposition reactions into competing stable phases are expressed as follows:

- $Hf_2ClC \rightarrow 0.5 \times Hf_2CCl_2 + 0.1 \times Hf_6C_5 + 0.4 \times Hf$
- $Hf_2BrC \rightarrow 0.5 \times Hf_2CBr_2 + 0.1 \times Hf_6C_5 + 0.4 \times Hf$

These competing phases were selected based on thermodynamic stability criteria and known structural feasibility. The calculated formation energies with respect to these phases are listed in Table 1. The negative values of the formation energies (ΔE_f in eV) confirm the relative stability of Hf_2ClC and Hf_2BrC, reinforcing the conclusions drawn from the formation enthalpy and binding energy analyses.

To further confirm the dynamical stability of Hf_2AC (A = Cl, Br) MAX phases, we conducted a phonon dispersion analysis at zero pressure and temperature. This evaluation is essential for determining the feasibility of synthesizing these compounds in a hexagonal structure. Using density functional perturbation theory (DFPT), we computed the phonon spectrum dispersion.[31]

The phonon dispersion curves (PDCs) with total density of states, shown in Fig. 2(a and b), offer vital information about stability. A fundamental criterion for dynamical stability is the absence of imaginary phonon frequencies in the dispersion curves. Since our results show no such imaginary frequencies, we confirm that Hf_2ClC and Hf_2BrC are dynamically stable and can potentially be synthesized experimentally.

Each graph displays three acoustic branches (red curves in the low-frequency region) and twenty-one optical branches (blue, green, and orange curves in the higher-frequency region). The longitudinal acoustic (LA) mode is seen progressing smoothly, while the transverse acoustic (TA) modes exhibit slight dispersion near the Γ-point. The transverse optical (TO) and longitudinal optical (LO) modes are located at higher frequencies for Hf_2ClC (~20 THz, ~15.35 THz) compared to Hf_2BrC (~19.22 THz, ~15.0 THz). This frequency reduction in Hf_2BrC is due to Br being heavier than Cl, which lowers the vibrational frequencies as per the inverse mass relation in lattice dynamics (*i.e.*, $\omega \propto 1/\sqrt{m}$). As a result, Hf_2BrC has softer optical phonon modes, leading to slightly lower phonon energy compared to Hf_2ClC. The low-frequency acoustic phonons (red curves), responsible for lattice vibrations and heat conduction, are slightly more dispersed in Hf_2BrC compared to Hf_2ClC. Since Br is larger than Cl, it weakens the bonding strength in Hf_2BrC, making the structure slightly more flexible. This results in lower acoustic phonon velocities, which could impact thermal conductivity. In both cases, the optical and acoustic phonon branches remain well-separated, which indicates limited phonon scattering. However, Br induces softer phonon modes compared to Cl. This may enhance acoustic–optical phonon interactions, leading to increased phonon scattering and reduced thermal conductivity. This suggests that Hf_2BrC might exhibit lower thermal conductivity than Hf_2ClC.

Hf_2AC (A = Cl, Br) MAX phases satisfy all essential stability criteria, including formation energy, phonon dispersion curves, and mechanical stability conditions (Section 3.3). These results confirm their thermodynamic and dynamical stability, making them strong candidates for experimental synthesis. Several MAX phases, including carbides, nitrides, and borides, have already been successfully synthesized.[41] Additionally, various Hf-based MAX phases, such as Hf_2AlC, Hf_3AlC_2, $Hf_5Al_2C_3$, Hf_2SnC, and Hf_3PbC_2 have been experimentally realized.[36,44–46] Given this trend, there is a strong potential for the successful synthesis of Hf_2ClC and Hf_2BrC, further expanding the family of Hf-based MAX phases.

3.3 Mechanical and elastic properties

Elastic constants are essential for evaluating the mechanical stability and stiffness of materials under external stress. The mechanical behavior of a crystal lattice is characterized by its second-order elastic stiffness constants, which play a crucial role in determining the mechanical stability of a material.[47] These constants are derived from the strain-energy relationship as:

$$C_{ij} = \frac{1}{V_0}\left(\frac{\partial^2 E}{\partial \varepsilon_i \partial \varepsilon_j}\right) \quad (3)$$

where E represents the energy of the crystal, V_0 is its equilibrium volume, and ε is the applied strain.

In hexagonal crystal structures, the stiffness matrix consists of 21 components, of which only six are independent: C_{11}, C_{12}, C_{13}, C_{33}, C_{44}, and C_{66}. Among these, C_{66} is dependent and follows the relation $C_{66} = (C_{11} - C_{12})/2$. The computed values of these elastic constants for Hf_2AC (A = Cl, Br) are presented in Table 2. To confirm mechanical stability, these values must satisfy the Born–Huang stability criteria for hexagonal structures:[47]

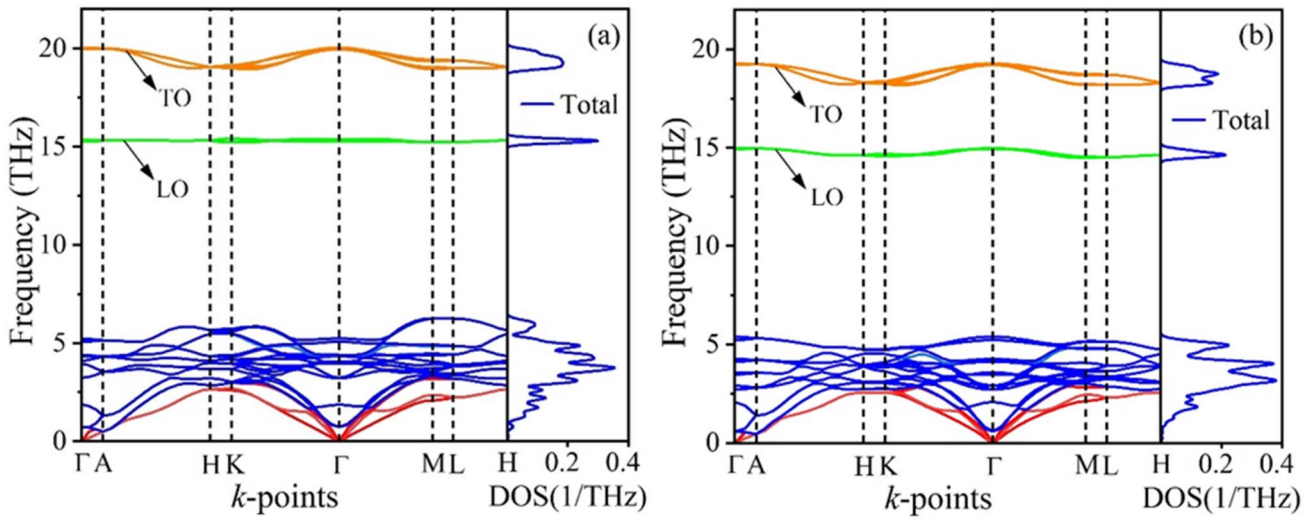

Fig. 2 Calculated phonon dispersion spectra and the right panel shows the phonon density of states for (a) Hf_2ClC, and (b) Hf_2BrC.

Table 2 The calculated stiffness constants (C_{ij} in GPa), Cauchy pressure (C'' in GPa), and Kleinman parameter (ζ) for Hf_2AC (A = Cl, Br) MAX phases along with some other theoretical results

Compounds	C_{11}	C_{12}	C_{13}	C_{33}	C_{44}	C_{66}	C''	ζ	Ref.
Hf_2ClC	165	56	75	140	27	54	29	0.48	This work
Hf_2BrC	156	78	68	147	22	39	56	0.63	
Hf_2AlC	329	70	81	272	126	129	−56	—	Ref. 23
Hf_2SC	320	95	121	330	149	113	−54	—	Ref. 34
Hf_2SnC	293	87	101	278	110	103	−23	—	Ref. 35
Hf_2TlC	278	69	62	230	71	104	−2	—	Ref. 33

$$C_{11} > |C_{12}|,\ 2C_{13}^2 < C_{33}(C_{11} + C_{12}),\ C_{44} > 0 \text{ and } C_{66} > 0 \quad (4)$$

The computed values for Hf_2ClC and Hf_2BrC meet these criteria, indicating that they are mechanically stable. These results suggest that these MAX phases can be considered for further experimental exploration. Since no prior experimental or theoretical data exist for the elastic constants of Hf_2ClC and Hf_2BrC, a comparative analysis with other Hf-based MAX phases provides valuable insights into their mechanical behavior.

A comparison of the stiffness constants in Table 2 reveals that Hf_2ClC and Hf_2BrC exhibit lower mechanical stiffness than other Hf-based MAX phases. The values of C_{11}, which represent resistance to uniaxial deformation, are 165 GPa and 156 GPa for Hf_2ClC and Hf_2BrC, respectively. These values are significantly lower than those of other Hf-based MAX phases, indicating that halogen-based MAX phases are more flexible. Similarly, the values of C_{33}, which represent resistance to compression along the *c*-axis, are 140 GPa for Hf_2ClC and 147 GPa for Hf_2BrC, compared to much higher values in Hf_2AlC, Hf_2SC, Hf_2SnC, and Hf_2TlC. This reduction in stiffness along the *c*-axis suggests that halogen substitution weakens bonding in this direction, making these structures more compliant under mechanical stress. The shear modulus, represented by C_{44} and C_{66}, is also significantly lower in Hf_2ClC (27 GPa, 54 GPa) and Hf_2BrC (22 GPa, 39 GPa) compared to other Hf-based MAX phases as mentioned in Table 2. This suggests that Hf_2ClC and Hf_2BrC have reduced resistance to shear deformation, with Hf_2BrC being even more flexible due to the larger atomic size and lower electronegativity of Br, which weakens the overall bonding strength.

The stiffness constants C_{ij} reveal the elastic anisotropy of Hf_2ClC and Hf_2BrC. The difference between C_{11} and C_{33} indicates stronger bonding along the *a*(*b*)-axis than the *c*-axis, making compression along the *a*-axis more difficult. The higher C_{11} value confirms that bonding along [100] is stronger than along [001], similar to other Hf-based MAX phases.[23,33–35] The lower C_{44} values suggest shear deformation is easier than linear compression, providing flexibility while maintaining structural integrity. The lower values of C_{12} and C_{13} compared to C_{11} and C_{33} indicate that stress along the *a*-axis significantly affects mechanical properties. The equation $C_{11} + C_{12} > C_{33}$ shows that the bonds are stronger bonding in the (001) plane than along the *c*-axis. The difference between two specific elastic constants, known as the Cauchy pressure, is expressed as $C'' = (C_{12} - C_{44})$ and serves as an indicator of a material's ductility or brittleness. A positive Cauchy pressure suggests ductility, while a negative value indicates brittleness. It also helps us understand how atoms bond in solids. A positive Cauchy pressure implies predominant ionic bonding, whereas a negative value suggests covalent bonding.[48] The positive C'' values for Hf_2ClC (29 GPa) and Hf_2BrC (56 GPa) (see in Table 2) confirm their ductile nature, which enhances their resistance to mechanical failure under stress. The presence of ionic bonding improves their flexibility, making them suitable for applications requiring high toughness, such as wear-resistant and impact-resistant coatings. Their ductile behavior also ensures better machinability, enabling their use in cutting tools and structural components exposed to cyclic loading. Additionally, their combination of ductility and moderate stiffness makes them promising for thermal barrier coatings, where resistance to thermal shock and mechanical integrity are crucial.

The substitution of Cl and Br in A site of Hf_2AC (A = Cl, Br) significantly affects the Kleinman parameter $\left(\zeta = \frac{C_{11} + 8C_{12}}{7C_{11} + C_{12}}\right)$, which describes the relative contributions of bond bending and bond stretching in response to mechanical deformation.[49] The Kleinman parameter is a dimensionless parameter that typically lies in the range $0 \leq \zeta \leq 1$. The calculated ζ values increase from 0.48 in Hf_2ClC to 0.63 in Hf_2BrC, indicating a shift toward greater bond bending dominance. This change is attributed to the larger atomic radius of Br, which weakens Hf–Br bonds compared to Hf–Cl, making it easier for bonds to bend rather than stretch under stress. A higher ζ value in Hf_2BrC suggests greater flexibility and the ability to absorb mechanical strain more effectively. This enhances its resistance to damage, making it suitable for applications requiring impact resistance and adaptability to thermal expansion. In contrast, the lower ζ in Hf_2ClC indicates a more balanced contribution of bond bending and stretching, resulting in higher stiffness and structural stability. This makes Hf_2ClC a better candidate for applications where mechanical strength and rigidity are prioritized over flexibility.

The polycrystalline elastic moduli, including the bulk modulus (B), shear modulus (G), Young's modulus (E), and Poisson's ratio (ν), were determined from the single-crystal elastic constants using the Voigt–Reuss–Hill (VRH) approximations.[50] The Voigt and Reuss equations provide the upper and lower bounds for these moduli, and Hill's approximation takes their average to define the polycrystalline properties. The bulk modulus is calculated as $B_H = (B_V + B_R)/2$, where B_V and B_R are the Voigt and Reuss bulk moduli, respectively. Similarly, the shear modulus is given by $G_H = (G_V + G_R)/2$.

Using these values, Young's modulus and Poisson's ratio are derived from the relationships $E = 9B_HG_H/(3B_H + G_H)$ and $\nu = 3B_H - 2\ G_H/2(B_H + G_H)$. The computed values for Hf_2ClC and Hf_2BrC, along with other MAX phases, are presented in Table 3 and shown in Fig. 3(b).

The bulk modulus (B) represents a material's resistance to uniform compression. From Fig. 3(b), it can be observed that

Table 3 The calculated values of polycrystalline elastic moduli (B, G, Y in GPa), Pugh's ratio (B/G), Poisson's ratio (ν), hardness parameters (H_{micro} and H_{macro} in GPa) and machinability index (μ_M) of Hf_2AC (A = Cl, Br) phases along with other theoretical data

Phases	B	G	E	B/G	ν	H_{micro}	H_{macro}	μ_M	Ref.
Hf_2ClC	97.90	37.51	99.78	2.61	0.33	4.24	2.43	3.62	This work
	110.86	45.24	119.48	2.45	0.32	5.42	—	—	Ref. 2
Hf_2BrC	98.62	31.44	85.27	3.13	0.35	3.02	0.95	4.52	This work
	116.38	29.45	81.47	3.95	0.38	2.29	—	—	Ref. 2
Hf_2AlC	154	122	297	0.79	0.19	—	—	—	Ref. 23
Hf_2SC	183	123	300	1.49	0.23	—	—	—	Ref. 34
Hf_2SnC	161	102	252	1.58	0.24	—	—	—	Ref. 35
Hf_2TlC	129	87	214	1.48	0.22	—	—	—	Ref. 33

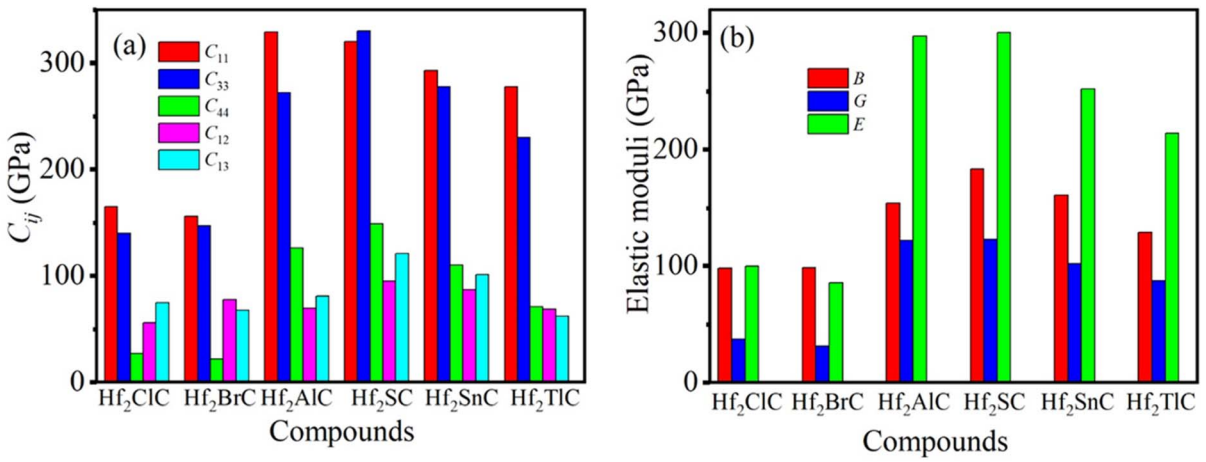

Fig. 3 Comparison of (a) elastic constants and (b) elastic moduli of Hf_2ClC and Hf_2BrC with other Hf-based MAX compounds.

Hf_2ClC (97.90 GPa) and Hf_2BrC (98.62 GPa) exhibit significantly lower bulk modulus (B) values compared to Hf_2AlC, Hf_2SC, Hf_2SnC and Hf_2TlC. This indicates that halogen-based MAX phases are more compressible and flexible. The lower B values suggest weaker interatomic bonding in Hf_2ClC and Hf_2BrC, making them more deformable under pressure. The bulk modulus (B) shows a slight increase of 0.73% upon Cl-to-Br substitution, indicating a minimal change in compressibility. This suggests that replacing Cl with the larger Br atom does not significantly alter the overall resistance to volumetric deformation. Despite this minor variation, both Hf_2ClC and Hf_2BrC remain highly compressible compared to other Hf-based MAX phases, reinforcing their potential for applications where flexibility and adaptability under mechanical stress are required.

The shear modulus (G), which measures resistance to shape deformation, is also lower in Hf_2ClC (37.51 GPa) and Hf_2BrC (31.44 GPa) compared to other Hf-based MAX phase.[23,33–35] This suggests that halogen-containing MAX phases have reduced resistance to shear forces, making them more ductile and less rigid than other Hf-based MAX phases. The value of G decreases significantly by 16.16% upon Cl-to-Br substitution, indicating that Hf_2BrC becomes more flexible and less resistant to shear deformation. This reduction in shear modulus can be attributed to the larger atomic radius and lower electronegativity of Br compared to Cl, which weakens interatomic bonding and reduces resistance to shear forces. The lower shear modulus enhances the material's ductility, making Hf_2BrC more adaptable under mechanical stress. The improved ductility makes Hf_2BrC suitable for environments subjected to mechanical shocks or vibrations, such as aerospace components and thermal barrier coatings.

Young's modulus (E), which defines the stiffness of a material, follows the same trend. This confirms that Hf_2ClC and Hf_2BrC are mechanically softer and more flexible compared to these Hf-based MAX phases.

The value of E decreases by 14.57% upon Cl-to-Br substitution, confirming reduced stiffness and structural rigidity in Hf_2BrC. This decline is primarily due to the weaker bonding strength introduced by the larger Br atoms, which reduce the overall bond strength and increase lattice flexibility. This reduction in stiffness enhances the material's toughness and damage tolerance, making Hf_2BrC a better candidate for applications requiring impact resistance and flexibility, such as protective coatings and shock-absorbing layers. The decreased E also suggests improved machinability, making it easier to process and shape for engineering applications.

In addition, Young's modulus (E) plays a crucial role in determining thermal shock resistance (R), as seen in the equation $R = \frac{\sigma_b(1-\nu)}{\alpha E}$, where σ_b stands for strength and α for thermal expansion coefficient.[51] A higher Young's modulus

leads to a lower thermal shock resistance, meaning materials with greater stiffness are more susceptible to thermal stress fractures. Since Hf_2BrC has a lower Young's modulus (85.27 GPa) compared to Hf_2ClC (99.78 GPa), it is expected to have better thermal shock resistance. This is because lower stiffness allows the material to absorb thermal stress more effectively, reducing the likelihood of crack propagation under rapid temperature changes. The greater thermal shock resistance of Hf_2BrC makes it a better candidate for these applications, as it can withstand sudden temperature variations without failure. On the other hand, Hf_2ClC, with its higher Young's modulus, may be more suitable for applications where structural rigidity and mechanical strength are prioritized over thermal shock resistance, such as load-bearing components in high-performance machinery.

The B/G ratio (Pugh's ratio) and Poisson's ratio (ν) are key indicators of a material's mechanical properties, particularly its brittleness or ductility.[52,53] The B/G ratio and Poisson's ratio (ν) of Hf_2ClC and Hf_2BrC are greater than those of other Hf-based MAX phases, as mentioned in Table 3. Generally, if $B/G > 1.75$, the material tends to be ductile, and if $B/G < 1.75$, it is more likely to be brittle. Both Hf_2ClC and Hf_2BrC have B/G ratios above 1.75, indicating they are ductile materials. However, Hf_2BrC shows a higher B/G ratio (3.13) compared to Hf_2ClC (2.61), suggesting it is slightly more ductile. This change is attributed to the larger ionic radius of Br compared to Cl, which allows for more flexible bonding and less rigidity in the structure, enhancing ductility.

Poisson's ratio (ν) reveals the compressibility, bonding forces, and nature of the material. The value of ν greater than 0.26 typically suggests ductility, while a value below 0.26 tends to indicate brittleness. Both values are above 0.26, indicating that both materials are ductile. The substitution of Cl with Br increases the Poisson's ratio slightly, which aligns with the trend seen in the B/G ratio and Cauchy pressure. This implies that the presence of Br in Hf_2BrC results in a slightly higher ductility compared to Hf_2ClC. This characteristic could make Hf_2BrC suitable for use in industries requiring durable, high-performance.

Moreover, the Poisson's ratio (ν) of Hf_2AC (A = Cl, Br) is critical in understanding the nature of the interatomic forces and the chemical bonding in these compounds. The values of ν for Hf_2ClC and Hf_2BrC are 0.33 and 0.35, respectively, both of which fall within the range of 0.25 to 0.50, indicating that the interatomic forces in these materials are central in nature.[49] This suggests that the material's deformation behavior is influenced by central forces between the atoms, rather than directional covalent forces.

The Poisson's ratio also gives an explanation for the bonding character. For purely covalent materials,[53] Poisson's ratio is typically around 0.10, while for purely ionic materials, it tends to be closer to 0.25. The calculated Poisson's ratios for Hf_2ClC and Hf_2BrC (both above 0.25) suggest that these compounds exhibit a significant ionic contribution to their chemical bonding. When considering the substitution of Cl with Br, the increase in Poisson's ratio from 0.33 to 0.35 (Hf_2ClC to Hf_2BrC) indicates a slight enhancement in the ionic bonding character. Br, being larger and less electronegative than Cl, may result in a more flexible atomic structure, which could lead to a slightly greater ionic interaction. This subtle increase in ionic bonding may contribute to Hf_2BrC's slightly greater ductility compared to Hf_2ClC, as reflected in its higher B/G ratio. Thus, the Cl-to-Br substitution slightly enhances the ionic character of the bonding in Hf_2BrC, which could improve its mechanical properties, making it more ductile.

The hardness of a material is a key factor in its ability to resist deformation, wear, and indentation under force. For Hf_2AC (A = Cl, Br) compounds, the hardness parameters (H_{micro}, H_{macro}) are calculated by following relation:[54,55]

$$H_{micro} = \frac{(1-2\nu)E}{6(1+\nu)} \quad (5)$$

$$H_{macro} = 2(k^2G)^{0.585} - 3 \quad (6)$$

where, k and G refers to Pugh's ratio ($k = G/B$) and shear modulus, respectively.

The calculated hardness values for Hf_2ClC (H_{micro} = 4.24 GPa, H_{macro} = 2.43 GPa) and Hf_2BrC (H_{macro} = 3.02 GPa, H_{micro} = 0.95 GPa) show that both compounds are relatively soft, with Hf_2BrC being softer than Hf_2ClC (see Table 3). The Cl-to-Br substitution in Hf_2AC (A = Cl, Br) leads to a reduction in hardness, with Hf_2BrC showing significantly lower hardness compared to Hf_2ClC. The lower hardness of Hf_2BrC can be attributed to the larger atomic size of Br compared to Cl, which likely results in weaker atomic bonds and a more easily deformable structure. The relatively soft nature of Hf_2ClC and Hf_2BrC makes these materials suitable for applications where high hardness is not a critical requirement, but good ductility and flexibility are desired. Additionally, Hf_2BrC, with its lower hardness, may find use in applications that require easier machining or shaping, such as in electronic components or catalysts where moderate mechanical strength suffices.

The machinability index ($\mu_M = B/C_{44}$) is an important parameter for assessing the plasticity and lubricating properties of a material.[56] It is influenced by factors such as elastic properties, hardness, and the ability of a material to undergo plastic deformation. A higher μ_M value indicates improved lubrication, reduced friction, and enhanced machinability, making the material easier to shape and process. The calculated values of μ_M for Hf_2ClC and Hf_2BrC are presented in Table 3, showing that Hf_2BrC has better machinability compared to Hf_2ClC. This is due to Br's larger atomic size, which weakens atomic bonding, increasing plasticity and easing deformation. Hardness and machinability are inversely related, meaning materials with lower hardness are generally easier to machine. The decrease in hardness for Hf_2BrC is 28.77% (microhardness) and 60.91% (macro-hardness), while its machinability index is 24.86% higher than Hf_2ClC. This confirms that as hardness decreases, machinability improves due to weaker atomic bonding, allowing for easier deformation. The higher machinability of Hf_2BrC makes it suitable for high-speed machining, reducing tool wear and processing costs.

3.4 Elastic anisotropy

In this study, we explore the elastic anisotropy of Hf_2AC (A = Cl, Br), which is crucial for understanding its mechanical behavior under various conditions. Elastic anisotropy influences plastic deformation, crack propagation, and stress tolerance. The crystal structure (see Fig. 1) reveals distinct atomic arrangements along the $a(b)$ and c directions, leading to differences in bond strength. The stiffness along $a(b)$ is represented by C_{11}, while the stiffness along c is denoted by C_{33}. Since $C_{11} \neq C_{33}$, this confirms anisotropy in mechanical properties. The shear anisotropic factors (A_1, A_2, A_3) provide insight into the bonding strength variations across different atomic planes. The shear anisotropy factor for {100} shear planes between [011] and [010] directions is,[57]

$$A_1 = \frac{4C_{44}}{C_{11} + C_{33} - 2C_{13}} \quad (7)$$

for {010} shear planes between [101] and [001] directions

$$A_2 = \frac{4C_{55}}{C_{22} + C_{33} - 2C_{23}} \quad (8)$$

for {001} shear planes between [110] and [010] directions

$$A_3 = \frac{4C_{66}}{C_{11} + C_{22} - 2C_{12}} \quad (9)$$

The calculated shear anisotropic factors of Hf_2AC (A = Cl, Br) are listed in Table 4. The calculated anisotropy values indicate that both Hf_2ClC and Hf_2BrC exhibit moderate anisotropy, with deviations from the ideal isotropic value (1). However, Cl-to-Br substitution significantly impacts the degree of anisotropy. For Hf_2BrC, A_1 and A_2 values decrease compared to Hf_2ClC, dropping from 0.69 to 0.52, indicating an increase in anisotropy in {100} and {010} shear planes. This suggests that Br's larger atomic size weakens directional bonding, leading to increased deformation along these planes. Despite these changes, A_3 remains 1.0 for both compounds, confirming isotropy in {001} plane. This comparison effectively highlights the practical implications of elastic anisotropy in Hf_2ClC and Hf_2BrC. Hf_2BrC's increased anisotropy suggests greater plastic deformation, making it more adaptable for flexible structural applications where some deformation can be tolerated. Conversely, Hf_2ClC's more uniform bonding structure enhances wear resistance and fracture toughness, making it more suitable for high-stress environments such as protective coatings or structural components.

We have also calculated the percentage elastic anisotropy in shear (A^G) and compression (A^B), the universal anisotropy factor (A^U), the equivalent Zener anisotropy factor (A^{eq}) by the following common relation[58,59] and their estimated values are displayed in Table 4.

$$A^B = (B_V - B_R)/(B_V + B_R) \quad (10)$$

$$A^G = (G_V - G_R) + (G_V + G_R) \quad (11)$$

$$A^U = \left(\frac{5G_V}{G_R}\right) + \left(\frac{B_V}{B_R}\right) - 6 \quad (12)$$

$$A^{eq} = \left(1 + \frac{5}{12}A^U\right) + \sqrt{\left(1 + \frac{5}{12}A^U\right)^2 - 1} \quad (13)$$

For an isotropic crystal, $A^B = A^G = 0$. However, the degree of anisotropy is represented by any variation larger than zero. For both materials, the percent elastic anisotropy in compression (A^B) is 0.0, meaning they are isotropic in compressibility, implying uniform bulk modulus distribution. However, the percentage elastic anisotropy in shear (A^G) is 0.049 for Hf_2ClC and 0.045 for Hf_2BrC, confirming slight anisotropy in shear deformation. The lower A^G value for Hf_2BrC suggests that Br substitution weakens the directional dependency of shear modulus, slightly reducing anisotropy in shear compared to Cl.

Ranganathan and Ostoja-Starzewski[59] have introduced the concept of the universal elastic anisotropic index (A^U) which is a widely used index for determining anisotropy due to its capacity to be applied to all potential crystal symmetries. The crystal is completely isotropic when the value of the universal anisotropy index (A^U) is exactly equal to zero ($A^U = 0$). The universal anisotropy factor (A^U) values of 0.52 (Hf_2ClC) and 0.48 (Hf_2BrC) further indicate that both compounds deviate from perfect isotropy. Hf_2BrC has a slightly lower A^U value, signifying that the introduction of Br reduces overall elastic anisotropy.

For an isotropic crystal, the equivalent Zener anisotropy factor is equal to one ($A^{eq} = 1$). The equivalent Zener anisotropy factor (A^{eq}) values of 1.91 (Hf_2ClC) and 1.86 (Hf_2BrC) support this trend, confirming moderate anisotropy. Br substitution weakens atomic bonding, which makes the material less stiff in one direction and a little more flexible in another. This makes Hf_2BrC more adaptable for applications requiring flexibility, while Hf_2ClC remains preferable for high-stress applications requiring superior mechanical stability.

The compressibility ratio $\left(k_c/k_a = \frac{C_{11} + C_{12} - 2C_{13}}{C_{33} - C_{13}}\right)$ provides insight into how a material deforms under stress along different crystallographic directions.[60] A higher ratio indicates greater compressibility along the c-axis compared to the a-axis,

Table 4 The calculated shear anisotropic factors (A_1, A_2 and A_3), percentage anisotropy in the compression and shear (A^B and A^G), universal anisotropic index (A^U), equivalent Zener anisotropic factor (A^{eq}), compressibility ratio (k_c/k_a), and universal log-Euclidean index (A^L) for studied compounds Hf_2AC (A = Cl, Br)

Compounds	A_1	A_2	A_3	A^B	A^G	A^U	A^{eq}	k_c/k_a	A^L	Ref.
Hf_2ClC	0.69	0.69	1.0	0.0	0.049	0.52	1.91	2.38	1.27	This work
Hf_2BrC	0.52	0.52	1.0	0.0	0.045	0.48	1.86	2.12	1.08	

signifying directional anisotropy in response to external forces. For Hf_2ClC, k_c/k_a is 2.38, while for Hf_2BrC, it is 2.12 (see Table 4). This suggests that Hf_2ClC exhibits greater compressibility along the *c*-axis, making it more adaptable to deformation in this direction under applied stress. The substitution of Cl with Br in Hf_2AC (A = Cl, Br) leads to a decrease in the compressibility ratio (k_c/k_a) from 2.38 to 2.12, indicating an 11% reduction. This suggests that Hf_2BrC has lower anisotropy in compressibility compared to Hf_2ClC. Br is larger than Cl, so it doesn't weaken the bonding along the *c*-axis as much as Cl does. This makes the compressibility between the *a*- and *c*-axes more even. As a result, Hf_2BrC exhibits a more balanced mechanical response and improved structural stability under stress. On the other hand, Hf_2ClC, with its higher k_c/k_a ratio, is more compressible along the *c*-axis, making it more flexible and adaptable to deformation in this direction.

We have also calculated the universal log-Euclidean index (A^L) can be defined using the log-Euclidean formula.[58]

$$A^L = \sqrt{\left[\ln\left(\frac{B_V}{B_R}\right)\right]^2 + 5\left[\ln\left(\frac{C_{44}^V}{C_{44}^R}\right)\right]^2} \quad (14)$$

where, the subscripts V and R represent the Voigt and Reuss approximations, respectively. For the universal log-Euclidean index calculation, the Voigt and Reuss values of C_{44} are obtained from ref. 58 which are $C_{44}^V = [C_{44}^R + (3/5)((C_{11} - C_{12} - 2C_{44})^2/(3(C_{11} - C_{12}) + 4C_{44}))]$, and $C_{44}^R = [(5/3)((C_{44}(C_{11} - C_{12}))/3(C_{11} - C_{12}) + 4C_{44})]$.

The universal log-Euclidean index (A^L) for Hf_2ClC and Hf_2BrC is 1.27 and 1.08, respectively, indicating a 15% reduction with Br substitution. Since most crystalline solids have $A^L <$ 1.0, both compounds exhibit significant anisotropy, with Hf_2ClC being more anisotropic. The higher A^L and compressibility ratio (k_c/k_a) in Hf_2ClC (2.38) compared to Hf_2BrC (2.12) reflects its stronger layered character and pronounced anisotropic mechanical behavior. Br substitution weakens interlayer bonding due to its larger atomic radius, leading to a more uniform elastic response and reduced anisotropy in Hf_2BrC. This translates to enhanced structural flexibility and adaptability, making Hf_2BrC suitable for applications requiring moderate mechanical compliance. In contrast, Hf_2ClC, with its higher anisotropy and directional bonding, is suitable for high-stress environments where mechanical rigidity is crucial.

Thus, replacing Cl with Br reduces anisotropy, balancing structural properties and making Hf_2BrC a more isotropic material with improved mechanical versatility.

3.5 Thermo-mechanical properties

In the study of acoustics for crystalline solids, sound velocity is a critical parameter, especially in elastically anisotropic materials where sound velocities vary depending on the direction in which elastic waves propagate. These materials exhibit different velocities for longitudinal and transverse waves, which are key in understanding their mechanical, electrical, and thermal conductivities. The sound velocity is directly related to the material's elastic moduli and can be calculated using the longitudinal (v_l) and transverse (v_t) sound velocities. The average sound velocity, v_a, is derived from the following formula:[61]

$$v_a = \left[\frac{1}{3}\left(\frac{2}{{v_t}^3} + \frac{1}{{v_l}^3}\right)\right]^{-\frac{1}{3}} \quad (15)$$

where the transverse sound velocity v_t is given by:

$$v_t = \sqrt{G/\rho} \quad (16)$$

And the longitudinal sound velocity v_l is:

$$v_l = \sqrt{(3B + 4G)/3\rho} \quad (17)$$

Acoustic impedance (Z) of a medium is another important parameter that can be calculated from its density (ρ) and shear modulus (G):[49]

$$Z = \sqrt{\rho G} \quad (18)$$

Higher acoustic impedance values are observed in denser and stiffer materials. The unit of acoustic impedance is Rayl (1 Rayl = 1 kg m^{-2} s^{-1} = 1 Ns m^3).

Finally, the radiation intensity (I) is also an important acoustical factor. It is proportional to the surface velocity of the material and scales with its density and modulus of rigidity. The radiation intensity can be expressed as:[49]

$$I \approx \sqrt{G/\rho^3} \quad (19)$$

The calculated values of sound velocities, acoustic impedance, and radiation factor for Hf_2AC (A = Cl, Br) are listed in Table 5 along with some other theoretical results. The substitution of Cl with Br in Hf_2AC (A = Cl, Br) significantly affects its acoustic properties due to the difference in atomic mass and bonding strength. The mass density increases from 10.17 g cm^{-3} in Hf_2ClC to 10.53 g cm^{-3} in Hf_2BrC, primarily due to the larger atomic weight of Br. This increase in density leads to a noticeable reduction in sound velocities. The transverse sound velocity decreases from 1921 m s^{-1} in Hf_2ClC to 1729 m s^{-1} in Hf_2BrC, reflecting a 10% reduction, while the longitudinal sound velocity drops from 3814 m s^{-1} to 3654 m s^{-1}, indicating a 4.2% decrease. The average sound velocity also declines by approximately 9.7%, from 2154 m s^{-1} to 1945 m s^{-1}, which suggests that the propagation of sound waves through the material becomes slower with Br substitution. Materials with lower acoustic radiation and slower phonon

Table 5 The calculated mass density (ρ in gm cm^{-3}), sound velocities (v_t, v_l and v_a in ms^{-1}), acoustic impedance (Z in Rayl), radiation factor (I in m^4 kg^{-1} s^{-1}) for Hf_2AC (A = Cl, Br)

Compounds	ρ	v_t	v_l	v_a	Z (10^6)	I	Ref.
Hf_2ClC	10.17	1921	3814	2154	19.53	0.19	This work
Hf_2BrC	10.53	1729	3654	1945	18.21	0.16	
Hf_2AlC	9.65	3560	5730	3920	—	—	Ref. 23
Hf_2SC	11.02	3840	5300	3740	—	—	Ref. 34
Hf_2TlC	13.04	2589	4345	2866	—	—	Ref. 33

Table 6 The calculated values of Debye temperature (Θ_D in K), melting temperature (T_m in K), thermal expansion coefficient (α in K^{-1}), heat capacity (ρC_P in J m^{-3} K^{-1}), Grüneisen parameter (γ), dominant phonon wavelength (λ_{dom} in m), minimum thermal conductivity (k_{min} in W m^{-1} K^{-1}) and lattice thermal conductivity (k_{ph} in W m^{-1} K^{-1} at 300 K) for Hf_2AC (A = Cl, Br)

Compound	Θ_D	T_m	γ	k_{ph}	k_{min}	α ($\times 10^{-5}$)	ρC_P ($\times 10^{6}$)	λ_{dom} ($\times 10^{-12}$)
Hf_2ClC	250	1059	1.98	2.61	0.722	4.27	2.51	89.51
Hf_2BrC	221	1044	2.18	1.65	0.630	5.09	2.33	81.10

propagation tend to have lower thermal conductivity, making them suitable for thermal insulation or thermal barrier coatings. Additionally, because they minimize energy loss from lattice vibrations, they can enhance the efficiency and durability of devices operating at high temperatures or under thermal stress. Substituting Br for Cl increases density, slows sound propagation, and reduces acoustic radiation, making Hf_2BrC better at damping vibrations and insulating heat, which is advantageous for high-temperature and thermal barrier applications.

Furthermore, the acoustic impedance, which measures a material's ability to transmit sound, decreases from 19.53 $\times$ 10^6 Rayl in Hf_2ClC to 18.21 $\times$ 10^6 Rayl in Hf_2BrC, showing a 6.8% reduction. This suggests that Hf_2BrC exhibits weaker impedance matching, making it less effective in transmitting sound. Additionally, the radiation factor, which indicates a material's ability to radiate sound energy efficiently, decreases by 15.8%, from 0.19 to 0.16 m^4 kg^{-1} s^{-1}. The reduction in both acoustic impedance and radiation efficiency implies that Hf_2BrC has weaker bonding interactions and a lower capacity to propagate and radiate sound compared to Hf_2ClC. Overall, Cl-to-Br substitution results in a material with reduced sound transmission and increased structural flexibility, making Hf_2BrC more suitable for applications requiring lower acoustic impedance, while Hf_2ClC remains preferable for high-speed acoustic applications.

In conclusion, the incorporation of halogens like Cl and Br in Hf_2AC compounds leads to a reduction in sound velocities and mechanical stiffness compared to other hafnium-based materials, as shown in Table 5. This suggests that these halogen-substituted compounds may exhibit more flexibility or adaptability under certain conditions.

3.6 Thermo-lattice properties

The Debye temperature (Θ_D) is a crucial thermophysical parameter that provides significant insights into the thermal and mechanical behavior of materials. It is related to the material's lattice vibrations, thermal conductivity, interatomic bonding, and other properties such as melting temperature and specific heat capacity. The Debye temperature effectively serves as a cutoff for the phonon energy distribution and helps distinguish between the classical and quantum mechanical behavior of phonons. The values of Θ_D are obtained from the following equation:[62]

$$\Theta_D = \frac{h}{k_B}\left[\left(\frac{3n}{4\pi V_0}\right)\right]^{1/3} v_a \quad (20)$$

where h is Planck's constant, n is the number of atoms in the unit cell, k_B is the Boltzmann constant, and V_0 is the equilibrium volume. The Debye temperature (Θ_D) for Hf_2ClC is 250 K, while for Hf_2BrC, it is 221 K are listed in Table 6. This shows a reduction of approximately 11.6% in the Debye temperature when Cl is replaced with Br. The decrease in the Debye temperature suggests that the interatomic bonding in Hf_2BrC is weaker than in Hf_2ClC. This results in less efficient lattice vibrations and lower mechanical wave velocities in Hf_2BrC compared to Hf_2ClC. The reduced Debye temperature in Hf_2BrC indicates that the material has a lower thermal conductivity due to weaker atomic interactions. This behavior can be attributed to the larger atomic radius of Br compared to Cl, which introduces more spacing between the atoms, weakening the bonding and lowering the lattice thermal conductivity. These weaker atomic interactions in Hf_2BrC result in a lower Debye temperature and reduced thermal conductivity. In contrast, Hf_2ClC, with its stronger atomic interactions, is expected to exhibit a higher lattice thermal conductivity. The stronger bonds in Hf_2ClC allow for more efficient heat transfer through the crystal lattice. Therefore, the substitution of Cl with Br reduces the atomic bonding strength, leading to lower thermal conductivity in Hf_2BrC compared to Hf_2ClC.

The melting temperature[63] ($T_m = 354 + 1.5\ (2C_{11} + C_{33})$), of a material is a key thermophysical property that reflects the strength of atomic interactions and the material's thermal stability. For Hf_2ClC, the calculated melting temperature is 1059 K, while for Hf_2BrC, it is 1044 K. This difference indicates a 1.4% decrease in the melting temperature when Cl is substituted with Br. The lower melting temperature in Hf_2BrC can be attributed to the relatively weaker atomic interactions compared to Hf_2ClC. As previously discussed, Br atoms are larger than Cl atoms, which increases the interatomic spacing and weakens the bonds between atoms. The correlation between melting temperature and Young's modulus (E) also supports this observation. A higher Young's modulus typically indicates stronger atomic bonding and greater material stiffness.

The Grüneisen parameter $\left(\gamma = \frac{3}{2}\left(\frac{1+\nu}{2-3\nu}\right)\right)$ is an essential measure of anharmonic effects in crystalline solids, influencing thermal expansion, phonon interactions, and thermomechanical properties.[64] Grüneisen parameters for different polycrystalline materials are within the expected range [0.85–3.53] with the Poisson's ratio in the range of 0.05–0.46 which are good agreement with our calculated values.[64] The calculated values for Hf_2ClC and Hf_2BrC are 1.98 and 2.18, respectively,

indicating that Hf_2BrC exhibits a higher degree of anharmonicity than Hf_2ClC. The 10.1% increase in the Grüneisen parameter when Cl is replaced with Br suggests that the lattice vibrations in Hf_2BrC are more sensitive to temperature changes and exhibit stronger anharmonic interactions. Additionally, the reduction in Debye temperature (by 11.6%) and melting temperature (by 1.4%) in Hf_2BrC further supports the trend of increased anharmonicity, as lower bond strength and structural rigidity contribute to greater phonon–phonon interactions.

Lattice thermal conductivity (k_{ph}) is one of the most fundamental and crucial properties of a material, especially for high-temperature applications, and describes how efficiently heat is conducted through phonon propagation inside a crystal. For Hf_2ClC and Hf_2BrC compounds, lattice thermal conductivity (κ_{ph}) is estimated at 300 K using Slack's formula:[65]

$$k_{ph} = A(\gamma)\frac{M_{av}\theta_D{}^3\delta}{\gamma^2 n^{2/3} T} \quad (21)$$

Here, M_{av} is the average atomic mass (in kg mol^{-1}), δ is the cubic root of the average atomic volume (in units of m^3), n is the number of atoms per unit cell, T is the absolute temperature, γ is the Grüneisen parameter, and A is a factor (in W-mol kg^{-1} m^{-2} K^{-3}) dependent on γ. The coefficient $A(\gamma)$ in Slack's model is determined by Julian's equation:[66]

$$A(\gamma) = \frac{5.72 \times 10^7 \times 0.849}{2 \times (1 - 0.514/\gamma + 0.228/\gamma^2)} \quad (22)$$

The calculated values of lattice thermal conductivities at room temperature under study are listed in Table 6. The k_{ph} value of Hf_2ClC and Hf_2BrC at 300 K is 2.61 W mK^{-1} and 1.65 W mK^{-1}, respectively, indicating a significant reduction of approximately 36.8% when Cl is substituted with Br. This reduction in thermal conductivity aligns with the observed decrease in Debye temperature, as lower Debye temperatures correlate with weaker interatomic bonding and reduced phonon propagation efficiency. The larger Br atomic radius increases spacing, enhancing phonon scattering and reducing lattice thermal conductivity. As a result, Hf_2BrC exhibits greater thermal insulation properties compared to Hf_2ClC, making it a more suitable candidate for applications requiring thermal barrier coatings and thermoelectric materials. Conversely, Hf_2ClC, with its higher thermal conductivity, is better suited for heat dissipation applications in microelectronic and nanoelectronic devices.

The lattice thermal conductivity of a compound approaches a minimal value at high temperatures above the Debye temperature, which is known as minimum thermal conductivity (k_{min}), which is independent of further increasing temperature. The minimum thermal conductivity estimated by using the following equation:[67]

$$k_{min} = k_B\left[\frac{nN_A\rho}{M}\right]^{2/3} v_a \quad (23)$$

where M is molar mass, and N_A is Avogadro's number.

The minimum thermal conductivity (k_{min}) of Hf_2ClC is 0.722 W mK^{-1}, while for Hf_2BrC, it is 0.630 W mK^{-1}, indicating a decrease of approximately 12.7% when Cl is replaced by Br. Since k_{min} is closely related to sound velocity and Debye temperature, the lower values in Hf_2BrC suggest that it has weaker atomic interactions and a less rigid lattice compared to Hf_2ClC. The minimum thermal conductivity of the studied MAX phase compounds, Hf_2ClC and Hf_2BrC, is significantly lower than the reference value of 1.25 W mK^{-1}, making them suitable candidates for thermal barrier coatings (TBC) applications. The lower k_{min} values indicate that these materials exhibit limited heat conduction at elevated temperatures, an essential property for TBCs used in aerospace and energy applications.

The substitution of Cl with Br in Hf_2AC (A = Cl, Br) significantly affects the thermal expansion coefficient, volumetric heat capacity, and dominant phonon wavelength, leading to variations in thermal performance. The calculated values of these parameters are listed in Table 6. The thermal expansion coefficient[60] $\left(\alpha = \frac{1.6 \times 10^{-3}}{G}\right)$ of Hf_2BrC is higher than that of Hf_2ClC, indicating that Hf_2BrC undergoes greater expansion with increasing temperature. This increase is primarily attributed to the larger atomic radius of Br. Since the thermal expansion coefficient is inversely related to the melting temperature, the lower melting point of Hf_2BrC further supports this observation. In practical applications, a lower thermal expansion coefficient is desirable for thermal barrier coatings to prevent thermal stress and structural instability. Therefore, Hf_2ClC, with its lower expansion, is a more suitable candidate for coatings in high-temperature environments.

The volumetric heat capacity $\left(\rho C_P = \frac{3k_B}{\Omega}\right)$ of Hf_2ClC is higher than that of Hf_2BrC, suggesting that it has a greater ability to store thermal energy and maintain thermal stability.[49] A higher heat capacity results in lower thermal diffusivity and contributes to better thermal conductivity. Since heat capacity plays a crucial role in determining how well a material responds to temperature fluctuations, the higher value in Hf_2ClC aligns with its greater lattice thermal conductivity. This characteristic makes Hf_2ClC more effective in heat dissipation applications, such as microelectronics and aerospace coatings, where efficient thermal management is essential.

The dominant phonon wavelength $\left(\lambda_{dom} = \frac{12.566 v_a}{T} \times 10^{-12}\right)$ of Hf_2ClC is longer than that of Hf_2BrC, which indicates a higher average sound velocity and lower phonon scattering in the former.[49] A longer phonon wavelength facilitates heat transfer by reducing phonon–phonon interactions, leading to improved thermal conductivity. Conversely, the shorter phonon wavelength in Hf_2BrC implies increased phonon scattering, which hinders heat conduction and reduces thermal conductivity. This characteristic makes Hf_2BrC a potential candidate for thermal insulation and thermoelectric applications, where lower thermal conductivity is advantageous for energy conversion efficiency and thermal management.

Overall, the presence of Cl enhances thermal conductivity, stability, and lower expansion, making Hf_2ClC preferable for

applications requiring efficient heat dissipation and structural reliability. On the other hand, Br substitution increases phonon scattering and thermal expansion while reducing heat capacity, making Hf_2BrC more suitable for thermal insulation and thermoelectric applications.

3.7 Electronic properties

This section provides a detailed comparison of the electronic band structures of Hf_2ClC and Hf_2BrC, highlighting the effect of substituting Cl with Br. The calculated band structures of Hf_2ClC and Hf_2BrC are shown in Fig. 4(a and b). The band structure calculations, performed using the GGA-PBE approximation, span an energy range from −4.0 to 4.0 eV, with the Fermi level set at 0 eV. The computed band structures along high-symmetry directions in the Brillouin zone indicate that both materials exhibit metallic behavior, as evidenced by multiple bands crossing the Fermi level. The dispersive nature of the band structure along different crystallographic directions provides crucial insights into the electronic transport properties of Hf_2ClC and Hf_2BrC. The dispersion of energy bands along the *c*-direction (Γ–A, H–K, and M–L) and the *ab*-plane (A–H, K–Γ, Γ–M, and L–H) differs significantly due to variations in bonding strength and orbital hybridization. Along the *c*-direction (Γ–A, H–K, and M–L), the band dispersion is relatively weaker in both compounds, indicating higher electronic localization and lower mobility along this axis. The Mulliken population analysis reveals distinct bonding characteristics in Hf_2AC (A = Cl, Br) MAX phases (Table 7). Hf atoms exhibit small positive charges (+0.56*e* for Hf_2ClC and +0.21*e* for Hf_2BrC), while C atoms carry strongly negative charges (−0.85*e*), confirming substantial charge transfer from Hf to C and the presence of strong polar covalent Hf–C bonds within the layers. In contrast, the halogen atoms display different behaviors: Cl is slightly negative (−0.26*e*), indicating an ionic Hf–Cl interaction, whereas Br is slightly positive (+0.44*e*), reflecting a reversal in charge transfer. This reversal arises from Br's lower electronegativity and larger size, which weaken the ionic interaction and introduce a more covalent, polarizable Hf–Br bond. Consequently, interlayer bonding in Hf_2BrC is weaker, leading to enhanced ductility, reduced stiffness, and stronger anisotropic electronic behavior compared to Hf_2ClC. However, the effect of Cl and Br substitution is evident: in Hf_2ClC, the bands in these directions are slightly more dispersive than in Hf_2BrC, suggesting stronger interlayer coupling and better charge transport along the *c*-axis. Br has a larger atomic radius, which increases the space between layers. This reduces orbital overlap and makes the bands flatter, which lowers the electrical conductivity along the *c*-direction.

On the other hand, the bands along the *ab*-plane (A–H, K–Γ, Γ–M, and L–H) show stronger dispersion in both compounds. This means that charge transport in the plane is more efficient. This is due to the presence of stronger covalent interactions within the layers, particularly between Hf and C atoms. However, a noticeable difference exists between Hf_2ClC and Hf_2BrC: the bands in Hf_2ClC are more dispersive, suggesting enhanced electronic delocalization and lower effective mass of charge carriers in the *ab*-plane. This higher dispersion contributes to better electronic conductivity, making Hf_2ClC more suitable for electronic applications requiring high carrier mobility. In Hf_2BrC, the bands in the *ab*-plane are slightly flatter, implying increased carrier scattering and reduced conductivity due to weaker orbital interactions. Overall, the comparison of band dispersion along the *c*-direction and *ab*-plane reveals that Hf_2ClC has greater electronic transport properties, particularly within the layers, due to stronger hybridization and better orbital overlap. On the other hand, Hf_2BrC exhibits more localized electronic states, leading to higher effective mass and reduced carrier mobility, especially along the *c*-direction. These findings highlight the anisotropic electronic nature of these materials and their potential applications, with Hf_2ClC being more suitable for conductive applications and Hf_2BrC potentially offering advantages in thermal barrier coatings or electronic devices where controlled

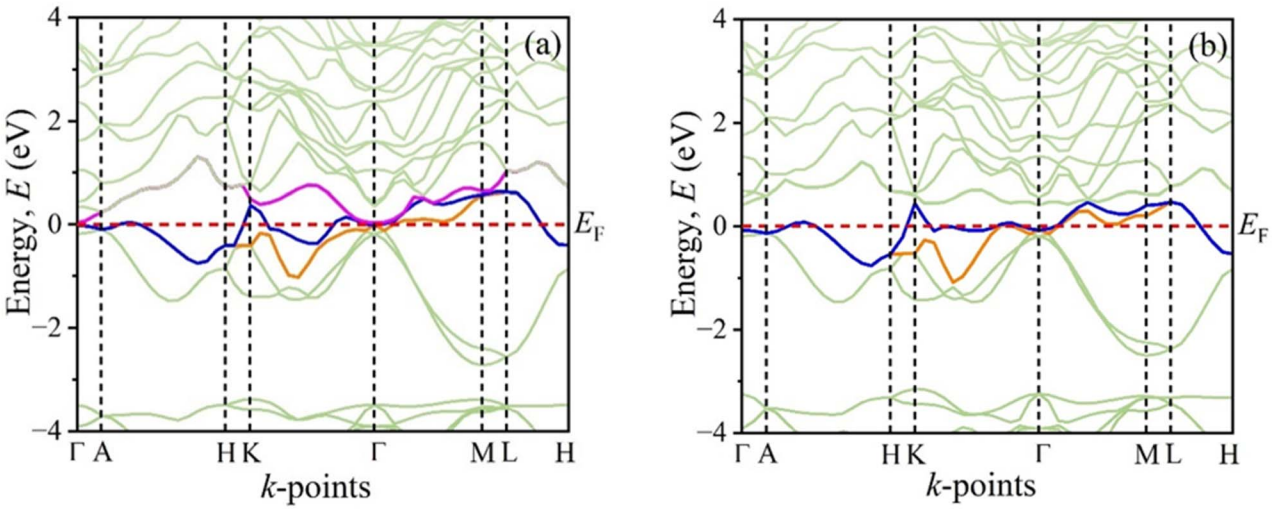

Fig. 4 Calculated band structure of (a) Hf_2ClC and (b) Hf_2BrC along the high symmetry directions in the Brillouin zone at ambient conditions.

Table 7 The calculated orbital charges (electron), atomic Mulliken charges (electron), effective valence (electron), and Hirshfeld charge (electron) of the Hf_2AC (A = Cl, Br) MAX compounds

		Mulliken atomic populations								
Compounds	Species	s	p	d	Total	Mulliken charge	Formal ionic charge	Effective valence	Hirshfeld charge	Effective valence
Hf_2ClC	C	1.53	3.33	0.0	4.85	−0.85	−4	3.15	−0.36	3.64
	Cl	1.93	5.34	0.0	7.26	−0.26	−1	0.74	0.03	0.97
	Hf	0.36	0.17	2.91	3.44	0.56	+4	3.44	0.17	3.83
Hf_2BrC	C	1.52	3.33	0.0	4.85	−0.85	−4	3.15	−0.36	3.64
	Br	1.31	5.25	0.0	6.56	0.44	−1	0.56	0.06	0.94
	Hf	0.43	0.47	2.90	3.79	0.21	+4	3.79	0.15	3.85

conductivity is required. The anisotropic transport observed in Hf_2AC (A = Cl, Br) aligns well with trends seen in other MAX phases.[5,7,68,69]

The density of states (DOS) plots in Fig. 5(a and b) provide deeper insight into the electronic structure of Hf_2ClC and Hf_2BrC, complementing the band structure analysis from Fig. 4. The variations in band dispersion along the *c*-direction (Γ–A, H–K, and M–L) and *ab*-plane (A–H, K–Γ, Γ–M, and L–H) can be directly linked to the differences in the projected DOS (PDOS) contributions of Hf, Cl, Br, and C atoms.

From Fig. 5(a and b), it is evident that the Hf-5d orbitals play a dominant role in the electronic states near the Fermi level (E_F). These orbitals are mainly responsible for the dispersive nature of the bands and charge transport characteristics. In Hf_2ClC, the Hf-5d states are more delocalized, contributing to the stronger dispersion observed in the band structure, particularly along the *ab*-plane, where covalent interactions between Hf and C are more prominent. This increased dispersion corresponds to lower effective mass and higher electronic mobility.

In contrast, in Hf_2BrC, the DOS shows that the Br-4p states contribute differently compared to Cl-3p states in Hf_2ClC. The Br-4p orbitals are more localized, leading to reduced hybridization with Hf-5d states. This weaker interaction results in flatter bands near the Fermi level, especially along the *c*-direction, where interlayer interactions are already weak. As a result, electronic conductivity is lower in Hf_2BrC compared to Hf_2ClC.

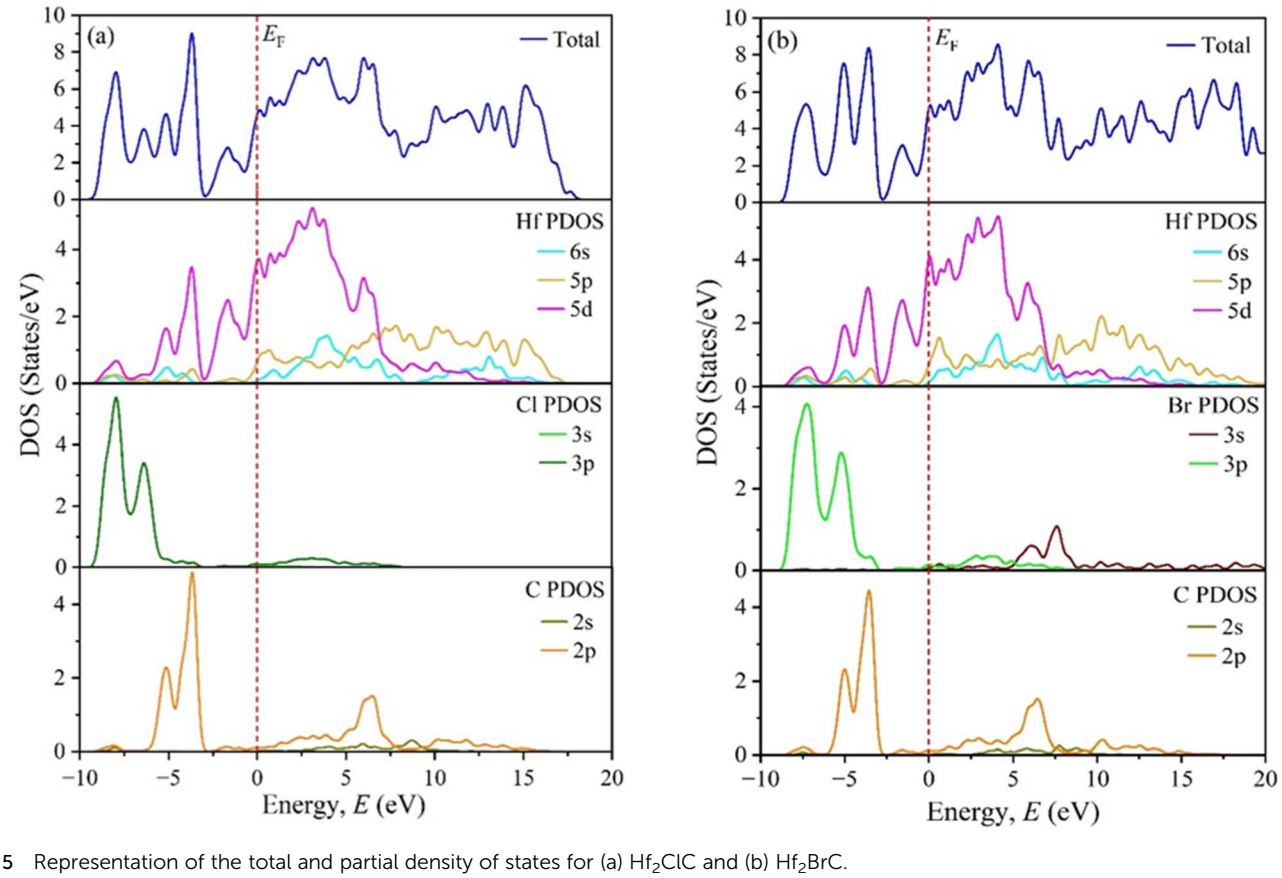

Fig. 5 Representation of the total and partial density of states for (a) Hf_2ClC and (b) Hf_2BrC.

The localization of Br states also has an effect on the dispersion along the *ab*-plane, but not as much as it does along the *c*-direction. Furthermore, the contribution of C-2p orbitals remains relatively similar in both compounds, indicating that variations in electronic dispersion are primarily influenced by the substitution of Cl with Br. The key factor in the observed differences in band dispersion is the reduced hybridization between Hf-5d and Br-4p states. Therefore, the DOS analysis confirms that the Hf-5d and halogen (Cl-3p or Br-4p) orbitals govern the band structure variations.

The electronic properties of Hf_2AC (A = Cl, Br) MAX phases are strongly influenced by their total density of states (TDOS), which plays a crucial role in assessing electrical stability. The calculated $N(E_F)$ values for Hf_2ClC and Hf_2BrC are 4.61 and 5.19 states per eV per unit cell, respectively. Lower $N(E_F)$ values indicate greater electrical stability, suggesting that Hf_2ClC is slightly more stable than Hf_2BrC. These values align with the stability range (2–12 states per eV per unit cell) found in other MAX phases, confirming the robust electrical stability of both materials.[70] A key feature in both compounds is the presence of a pseudo-gap near E_F, which separates bonding and anti-bonding states. The pseudo-gap functions as a barrier, restricting electron transitions and enhancing stability. The Fermi level lies within the bonding region, further supporting the stability of these structures. The substitution of Cl with Br slightly reduces the pseudo-gap, which correlates with a higher $N(E_F)$, leading to a minor decrease in stability for Hf_2BrC compared to Hf_2ClC. This modification occurs due to Br's larger atomic radius and lower electronegativity, which weaken the hybridization between Hf and A-site atoms, making electronic states more localized and reducing charge transport efficiency.

3.8 Charge density distribution map

The electronic charge density distribution maps for Hf_2ClC and Hf_2BrC reveal crucial insights into their chemical bonding and charge transfer characteristics. The color gradient in Fig. 6 illustrates the variation in electronic charge, with blue representing high charge density and red indicating low charge density. The substitution of Cl with Br influences the bonding nature within these MAX phases, affecting charge accumulation and hybridization.

Significant charge accumulation between Hf and C atoms in both compounds demonstrates strong covalent bonding between these atoms. This strong covalent character arises from the hybridization of Hf-5d and C-2p orbitals, which is consistent with the band structure and density of states (DOS) analysis. The substitution of Cl with Br does not significantly alter this Hf–C bonding, as it remains the dominant interaction in both materials. The Hf–A (A = Cl, Br) bonds also exhibit covalent character but are relatively weaker than Hf–C bonds. The electronic charge density around Cl and Br atoms is more localized, indicating weaker hybridization with Hf compared to Hf–C. The larger atomic radius and lower electronegativity of Br compared to Cl reduce the extent of orbital overlap with Hf, weakening the Hf–Br bond relative to Hf–Cl. This reduced bonding strength is also reflected in the flatter bands in the electronic band structure of Hf_2BrC, which suggests lower charge carrier mobility. A noticeable feature in the charge density maps is the ionic nature of Cl–C and Br–C bonds. In both compounds, there is a clear separation of charge between A-site (Cl/Br) and C atoms, confirming the ionic bonding character. However, the charge distribution around Br appears more diffuse compared to Cl, indicating a more polarized bond due to its larger size and lower

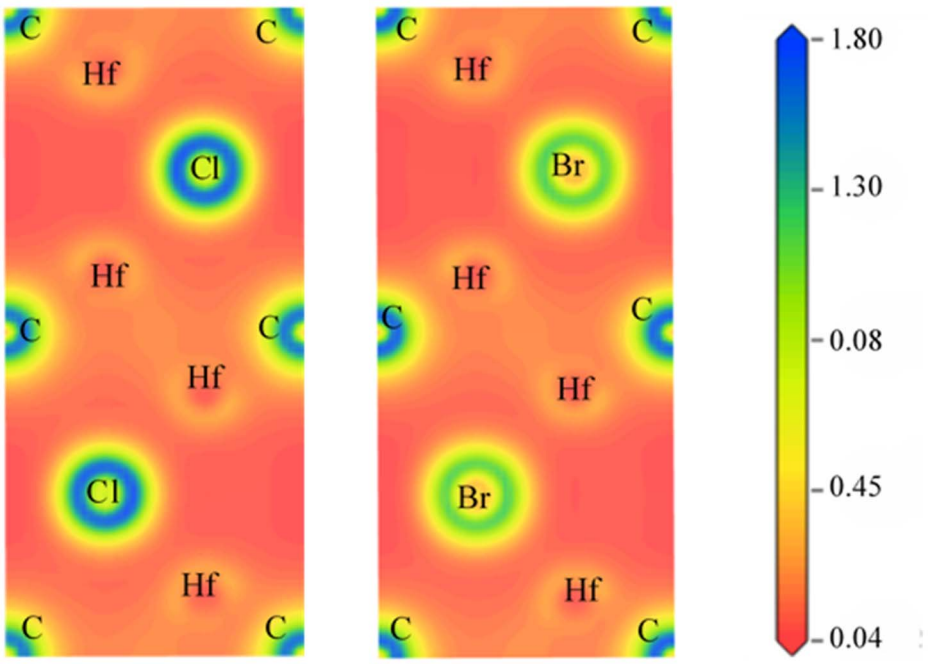

Fig. 6 Electronic charge density distribution map of Hf_2ClC (left) and Hf_2BrC (right), respectively.

electronegativity. This increased ionic nature further reduces the overall hybridization in Hf_2BrC, leading to a less dispersive electronic structure compared to Hf_2ClC.

3.9 Bond population analysis

The Mulliken atomic population analysis provides valuable insights into the nature of chemical bonding and charge transfer in Hf_2AC (A = Cl, Br) MAX compounds. The deviation of Mulliken charges from their formal ionic states indicates significant charge redistribution among the atoms, suggesting the coexistence of covalent and ionic bonding. The substitution of Cl with Br affects the charge transfer and bonding characteristics due to differences in electronegativity and atomic size between the two halogen elements.

In Hf_2ClC, the Mulliken charge on Cl is $-0.26e$, while in Hf_2BrC, Br exhibits a positive charge of 0.44e. This indicates that Br has a lower tendency to attract electrons compared to Cl, leading to weaker charge transfer in Hf_2BrC. The charge distribution also affects the bonding nature; Hf–Cl bonding exhibits stronger hybridization than Hf–Br, as reflected in the calculated effective valence charge (EVC). The EVC values for all species in both compounds are greater than zero, confirming the partial covalency of the bonds.[71] However, the effective valence of Hf in Hf_2BrC is slightly higher ($3.79e$) than in Hf_2ClC ($3.44e$), implying that the bonding in Hf_2BrC is less ionic and more covalent in nature. This phenomenon is primarily due to the larger atomic radius of Br, which reduces electrostatic attraction and weakens the bond strength between Hf and Br compared to Hf and Cl.

To further validate the bonding characteristics, the Hirshfeld population analysis (HPA) was performed, revealing variations from the Mulliken charge analysis.[72] Despite the differences, both methods consistently indicate that the Hf–C bonds remain predominantly covalent, while the Hf–Cl and Hf–Br bonds exhibit partial covalency with some ionic character. The Cl–C and Br–C bonds, however, are primarily ionic in both cases. The substitution of Cl with Br also affects electronic properties, as weaker bonding in Hf_2BrC leads to lower charge transfer efficiency and increased carrier localization. This results in reduced electronic conductivity and higher anisotropy in transport properties. However, the relatively weaker Hf–Br bonding may lead to a slight reduction in structural robustness compared to Hf_2ClC. Overall, the replacement of Cl with Br alters the bonding nature by decreasing the degree of charge transfer and reducing hybridization effects. This leads to a shift in electronic and transport properties, making Hf_2BrC slightly less ionic and more covalent but with weaker bonding interactions compared to Hf_2ClC.

3.10 Optical properties

The optical properties of materials are important because they determine their electronic nature and potential applications in optoelectronic devices, solar cells, lasers, photodetectors, sensors, and reconfigurable photonics. The optical behavior of Hf_2ClC and Hf_2BrC MAX phases is analyzed through the frequency-dependent complex dielectric function, $\varepsilon(\omega) = \varepsilon_1(\omega) + i\varepsilon_2(\omega)$, which directly correlates with the electronic structure across all photon energy levels.[73] The imaginary part $\varepsilon_2(\omega)$ can be calculated from the momentum matrix elements connecting to the occupied and unoccupied electronic states with the following relations:[74]

$$\varepsilon_2(\omega) = \frac{2e^2\pi}{\Omega\varepsilon_0}\sum_{k,v,c}\int |\psi_k{}^c\langle \hat{u}r\rangle\psi_k{}^v|^2\delta(E_k{}^c - E_k{}^v - E) \qquad (24)$$

where, the integral is over the first Brillouin zone, ω refers the frequency of light, e indicates the electronic charge, u is the vector indicating the polarization of the incident electric field, ε_0 is the dielectric constant in free space and $\Psi_k{}^c$ and $\Psi_k{}^v$ are the conduction and valence band wave functions respectively. The real part $\varepsilon_1(\omega)$ was obtained from the imaginary part $\varepsilon_2(\omega)$ by using the Kramer–Kronig (K–K) relations:[73]

$$\varepsilon_1(\omega) = 1 + \frac{2}{\pi}P\int_0^\infty \frac{\omega'\varepsilon_2\left(\omega'\right)\mathrm{d}\omega}{\left(\omega'^2 - \omega^2\right)} \qquad (25)$$

where P implies the principal value of the integral. In order to describe the material response to incident electromagnetic radiation, for studied MAX phase compounds Hf_2AC (A = Cl, Br) all the other energy-dependent optical parameters, like absorption coefficient $\alpha(\omega)$, photoconductivity $\sigma(\omega)$, loss function $L(\omega)$, reflectivity $R(\omega)$ and refractive index, $n(\omega)$ were computed directly from $\varepsilon_1(\omega)$ and $\varepsilon_2(\omega)$ and displayed in Fig. 7, respectively. These properties were examined across a photon energy range of up to 30 eV. As in the case of many MAX phases, Hf_2AC (A = Cl, Br) exhibits metallic behavior, which significantly influences their optical properties. The conduction electrons in these materials affect the dielectric function by changing how they respond to light. Specifically, the intra-band contributions from free electrons play a dominant role, affecting the low-energy optical spectrum. In metallic or metal-like conductors, both intra-band and inter-band transitions shape the optical behavior, requiring a precise approach for accurate characterization. To achieve a reliable analysis of the optical properties of Hf_2ClC and Hf_2BrC, the conventional Drude model was employed.[75] This model effectively accounts for free-electron contributions to the dielectric function. For our calculations, we incorporated a Drude damping parameter of 0.05 eV and a plasma frequency of 3 eV for both compounds. These values are consistent with earlier reports for metallic MAX phases and related carbides/nitrides,[76–80] where such parameters accurately describe the free-electron contributions and Drude-like behavior at low photon energies. The Drude term primarily captures the intra-band transitions, which dominate at low photon energies. These transitions arise due to the free-electron nature of the material and contribute significantly to optical conductivity, reflectivity, and absorption spectra.

3.10.1 Dielectric function. The optical behavior of Hf_2ClC and Hf_2BrC provides a compelling insight into their metallic nature, as depicted by the real $\varepsilon_1(\omega)$ and imaginary $\varepsilon_2(\omega)$ components of their dielectric function, which are depicted in Fig. 7(a and b). The presence of Cl and Br in these MAX phases leads to subtle yet significant differences in their optical

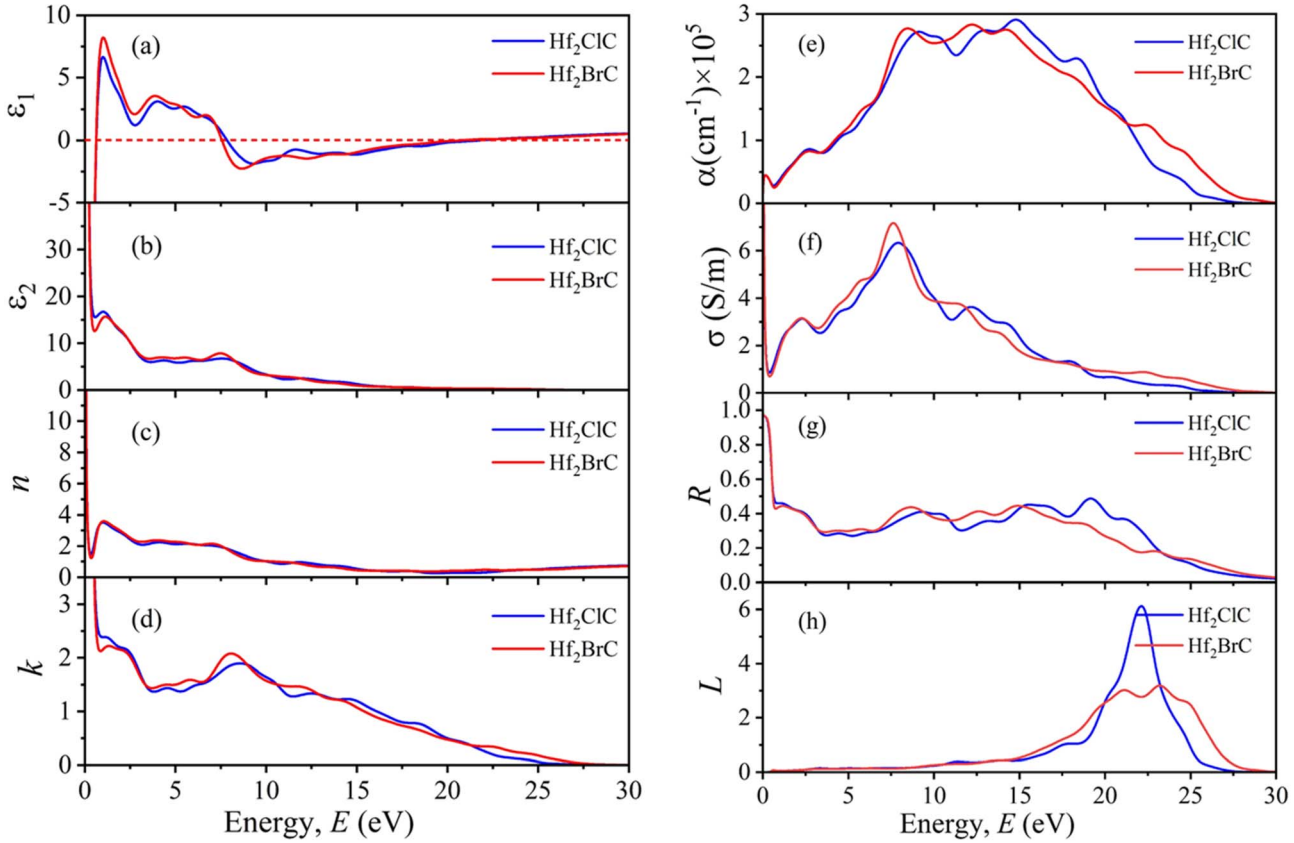

Fig. 7 The energy dependent (a) real part of dielectric function, (b) imaginary part of dielectric function, (c) refractive index, (d) extinction coefficient (e) absorption coefficient, (f) photoconductivity, (g) reflectivity, and (h) loss function of Hf_2ClC and Hf_2BrC, respectively.

responses. The real part $\varepsilon_1(\omega)$ exhibits a strong metallic character, showing negative values at low energy, which is consistent with the Drude-like behavior typically observed in conductive materials. This trend aligns well with the electronic band structure, reaffirming the metallic conductivity of these compounds. As shown in Fig. 7(a), $\varepsilon_1(\omega)$ attains large negative values at low photon energies and crosses zero at approximately 21.79 eV for Hf_2ClC and 20.77 eV for Hf_2BrC. This zero-crossing energy corresponds to the plasma frequency, where the absorption coefficient (Fig. 7(e)) vanishes, reflectivity (Fig. 7(g)) drops sharply, and the energy loss function (Fig. 7(h)) exhibits its first pronounced peak. Moreover, as depicted in Fig. 7(a) and (b), $\varepsilon_1(\omega)$ crosses zero from below and approaches zero from above, thereby reinforcing the metallic and highly reflective characteristics.

The imaginary part of the dielectric function, $\varepsilon_2(\omega)$, which represents optical absorption due to electron excitations, is shown in Fig. 7(b). The high $\varepsilon_2(\omega)$ values at low photon energies indicate strong absorption for both Hf_2ClC and Hf_2BrC. As seen in Fig. 7(b), $\varepsilon_2(\omega)$ initially drops to $\varepsilon_2 = 15.59$ at 0.57 eV for Hf_2ClC and to $\varepsilon_2 = 12.69$ at 0.56 eV for Hf_2BrC, before rising to their respective maxima of 16.84 at 0.97 eV and 15.65 at 1.13 eV. Beyond these peaks, $\varepsilon_2(\omega)$ gradually decreases almost exponentially across 1.38–6.49 eV and 8.24–15.77 eV for Hf_2ClC, and 3.35–7.93 eV for Hf_2BrC, reflecting their optical stability against excessive energy losses. The low-energy peaks originate from intra-band transitions of conduction electrons, while the high-energy peaks are attributed to inter-band transitions between occupied and unoccupied states, consistent with metallic characteristics. The high static dielectric constant of $\varepsilon_2(\omega)$ at low photon energies also signifies strong light–matter interactions, highlighting the potential of Hf_2ClC and Hf_2BrC for high-k dielectric, capacitor, and optical modulator applications.

3.10.2 Refractive index. The refractive index, $n(\omega)$, is a key optical parameter that governs how light propagates through a material, making it fundamental for photonic and optoelectronic applications. The variation of $n(\omega)$ with photon energy for Hf_2ClC and Hf_2BrC, shown in Fig. 7(c), exhibits a gradual decrease with increasing energy. Both compounds display remarkably high static refractive index values of $n(0) = 84.33$ for Hf_2ClC and 84.31 for Hf_2BrC, indicating strong light–matter interactions and high polarizability, which are advantageous for waveguides, photonic crystals, and energy-harvesting devices. The refractive index decreases sharply with photon energy, showing prominent peaks near 1.10 eV ($n = 3.58$) for both phases. Within the visible range (1.67–3.10 eV), $n(\omega)$ declines from 3.06 to 2.08 for Hf_2ClC and from 3.18 to 2.26 for Hf_2BrC. The slightly higher refractive index in Hf_2BrC can be attributed to Br's larger atomic radius and lower electronegativity, which modify the electronic structure and enhance polarization

effects. This tunable refractive response, combined with metallic conductivity, demonstrates the advantages of these MAX phases for advanced optoelectronic and photonic devices requiring efficient light modulation and energy management.

3.10.3 Extinction coefficient. The extinction coefficient, $k(\omega)$, a key optical parameter that quantifies the attenuation of electromagnetic radiation as it propagates through a material, reflects intrinsic absorption losses. This property provides valuable insight into light–matter interactions and is particularly significant for photonics, optical coatings, and optoelectronic device applications. The calculated $k(\omega)$ spectra for Hf_2ClC and Hf_2BrC, presented in Fig. 7(d), exhibit distinct frequency-dependent trends. As shown in Fig. 7(d), both compounds display high static values, $k(0) \approx 102.64$ for Hf_2ClC and 102.66 for Hf_2BrC, with strong absorption features in the infrared region. With increasing photon energy, $k(\omega)$ gradually decreases; however, Hf_2BrC reaches a slightly higher peak (k = 2.11 at 8.04 eV) compared to Hf_2ClC ($k = 1.88$ at 8.55 eV) in the visible range, indicating enhanced photon–electron coupling due to Br substitution. The pronounced extinction values signify efficient light absorption and strong photon-induced charge excitation, desirable for optical and photoactive devices. Additionally, $k(\omega)$ exhibits minor anisotropy within the 3.52–20.13 eV range, consistent with the layered structure of MAX phases. The observed local maxima in the $k(\omega)$ spectra coincide with the zero-crossing points of the real part of the dielectric function, confirming the correlation between energy loss and plasma resonance behavior.

3.10.4 Absorption coefficient. The absorption coefficient, $\alpha(\omega)$, provides vital information about a material's ability to absorb incident photon energy, directly influencing its optoelectronic performance. The absorption spectra of Hf_2ClC and Hf_2BrC, illustrated in Fig. 7(e), reveal strong photon–matter interactions extending across the infrared (IR), visible, and ultraviolet (UV) regions. Due to their metallic character, absorption begins at 0 eV and exhibits primary peaks at 0.18 eV ($\alpha = 0.46 \times 10^5$ cm^{-1}), followed by secondary peaks in the visible range near 2.69 eV, where α reaches approximately 0.84×10^5 cm^{-1} for both phases. Maximum absorption occurs in the UV region at 12.15 eV ($\alpha = 2.84 \times 10^5$ cm^{-1}) for Hf_2ClC and 14.79 eV ($\alpha = 2.91 \times 10^5$ cm^{-1}) for Hf_2BrC. Within the visible spectrum (1.67–3.10 eV), $\alpha(\omega)$ increases steadily from 0.61×10^5 cm^{-1} to 0.83×10^5 cm^{-1} for Hf_2ClC and from 0.59×10^5 cm^{-1} to 0.81×10^5 cm^{-1} for Hf_2BrC, indicating excellent light-harvesting efficiency. This consistent absorption behavior highlights the strong electronic transition activity within the conduction band, driven primarily by Hf-d orbital contributions near the Fermi level. The broad and intense absorption response across a wide energy range underscores the potential of these MAX phases for high-performance photodetectors, UV-visible absorbers, and other optoelectronic and photonic devices.

3.10.5 Photoconductivity. The photoconductivity spectra of Hf_2ClC and Hf_2BrC, illustrated in Fig. 7(f), commence at zero photon energy, confirming the absence of a band gap and thereby validating their metallic nature. This behavior arises from the presence of free charge carriers that contribute to electrical conductivity even at low photon energies. The observed trends in photoconductivity are consistent with the absorption coefficient, electronic band structure, and density of states (DOS) analyses, all of which indicate substantial carrier mobility and metallic behavior. The frequency-dependent optical conductivity, $\sigma(\omega)$, of Hf_2AC (A = Cl, Br) further highlights strong photon–electron interactions essential for charge transport processes. The static optical conductivity of these compounds is about 20.93 S m^{-1}, which means that they can move charges around easily and excite electrons quickly when light hits them. Within the visible region, $\sigma(\omega)$ varies between 2.77–2.59 S m^{-1} for Hf_2ClC and 2.82–2.75 S m^{-1} for Hf_2BrC, with the latter exhibiting slightly enhanced conductivity. The maximum photoconductivity is observed at 8.0 eV for Hf_2ClC (σ = 6.31 S m^{-1}) and at 7.67 eV for Hf_2BrC ($\sigma = 7.18$ S m^{-1}), after which $\sigma(\omega)$ decreases gradually with energy. The combination of strong low-energy conductivity and photon-induced carrier excitation underscores the potential of these MAX phases for optoelectronic and photoactive applications, including photodetectors, solar energy converters, and optical sensors, where efficient light-to-charge conversion is vital.

3.10.6 Reflectivity. The reflectivity spectra of Hf_2ClC and Hf_2BrC, presented in Fig. 7(g), exhibit similar overall trends, characteristic of metallic materials. Both compounds have high static reflectivity values of $R(0) \approx 0.98$, which shows that they are very good at reflecting low-energy electromagnetic radiation. As photon energy increases, the reflectivity decreases, reaching $R = 0.46$ at 0.82 eV for Hf_2ClC and $R = 0.43$ at 0.75 eV for Hf_2BrC. The spectra of both compounds follow a comparable decreasing trend up to approximately 3.44 eV, beyond which a slight anisotropy is observed, reflecting directional dependence in their optical response due to their layered crystal structure. Within the visible photon energy range (1.67–3.10 eV), Hf_2ClC and Hf_2BrC maintain moderate reflectivity levels between 43% and 32%, indicating controlled light reflection suitable for solar radiation management and optical coating applications. The high reflectivity in the low-energy region coupled with tunable optical anisotropy at higher energies suggests that these MAX phases could serve as efficient reflective coatings and thermal control materials for optoelectronic and high-temperature devices.

3.10.7 Loss function. The energy loss function, $L(\omega)$, represents the energy dissipated by fast-moving electrons traversing a material and provides critical insight into its plasmonic and dielectric behavior. As illustrated in Fig. 7(h), the $L(\omega)$ spectra for Hf_2ClC and Hf_2BrC exhibit no distinct peaks in the low-energy range (0–15 eV), which can be attributed to the relatively large values of the imaginary component of the dielectric function, $\varepsilon_2(\omega)$, that dampen collective oscillations. A prominent peak emerges between 15 and 28 eV for both compounds, corresponding to bulk plasma oscillations—collective excitations of conduction electrons within the material. The maximum peak in each spectrum indicates the bulk plasma frequency, where the real part of the dielectric function crosses zero, marking the transition from metallic to dielectric behavior. The calculated plasma frequencies are 22.21 eV for Hf_2ClC and 22.35 eV for Hf_2BrC, indicating a slightly stronger

plasmonic response in the Br-substituted phase. These energy-loss peaks coincide with sharp decreases in reflectivity, signifying the point at which the material transitions from a reflective to a transparent regime. Beyond the plasma frequency, both compounds exhibit minimal energy loss and increased transparency, suggesting their potential for high-frequency optical and plasmonic applications where low optical damping and efficient charge oscillations are essential.

4. Conclusions

This first-principles study reveals that A-site halogen substitution is an effective approach for tailoring the multifunctional behavior of Hf_2AC (A = Cl, Br) MAX phases. Both Hf_2ClC and Hf_2BrC phases are confirmed to be structurally, mechanically, and dynamically stable. The substitution of Cl with Br reduces stiffness, hardness, and sound velocity, enhancing ductility, vibration damping, and thermal insulation performance, suitable for thermal barrier applications. In contrast, Hf_2ClC exhibits greater rigidity, higher conductivity, and superior thermal dissipation, making it better suited for structural and heat-management uses. Electronically, both compounds display metallic conductivity dominated by Hf–C bonding, while optically, Br substitution shifts the absorption toward lower energies, improving infrared and UV responsiveness. Overall, halogen engineering at the A-site emerges as a powerful strategy for tuning mechanical, thermal, and optical functionalities in Hf-based MAX phases for diverse high-temperature and optoelectronic applications.

Author contributions

Asif Mohammed Arfi: investigation, methodology, data curation, conceptualization, writing original manuscript; Mahamudun Nabi: writing – original draft, methodology, formal analysis, data calculations, validation. Md. Hasan Mia: writing – original draft, review & editing, conceptualization, formal analysis, validation, supervision. Omar Alsalmi: data curation, formal analysis, review – editing; Muhammad Athar Uddin data curation, formal analysis, review – editing; Md. Zahid Hasan: formal analysis, validation, supervision, review – editing.

Conflicts of interest

The authors declare that they have no known conflicting financial interests or personal ties that may have seemed to affect the work presented in this study.

Data availability

Relevant data from this study are available from the corresponding author upon a reasonable request.

Acknowledgements

The authors extend their appreciation to Umm Al-Qura University, Saudi Arabia for funding this research work through grant number: 25UQU4300099GSSR10. Funding statement: This research work was funded by Umm Al-Qura University, Saudi Arabia under grant number: 25UQU4300099GSSR10.

References

1 M. A. Hadi, Superconducting phases in a remarkable class of metallic ceramics, *J. Phys. Chem. Solid.*, 2020, **138**, 109275.
2 D. Ohmer, Q. Gao, I. Opahle, H. K. Singh and H. Zhang, High-throughput design of 211-M 2 AX compounds, *Phys. Rev. Mater.*, 2019, **3**(5), 053803.
3 I. Ouadha, R. Habib, A.-R. Ahmed, A. Reggad and D. Rached, Study of the structural, mechanical and thermodynamic properties of the new MAX phase compounds (Zr1-xTix) 3AlC2, *Comput. Condens. Matter*, 2020, **23**, e00468.
4 A. Rached, H. R. Ahmed, M. Haque Babu, T. Hadji and D. Rached, Prediction of double transition metal (Cr1−xZrx) 2AlC MAX phases as thermal barrier coatings: Insight from density functional theory, *Int. J. Quant. Chem.*, 2021, **121**(20), e26770.
5 M. H. Mia, U. Ahmed, S. K. Saha and Md A. Ali, Unveiling mechanical, electronic, and optical properties of newly synthesized Mo2VAlC2 and Mo2V2AlC3 o-MAX phases via first-principles calculations, *J. Mater. Res. Technol.*, 2025, **36**, 2468–2484.
6 Y. Katoh, L. L. Snead, T. Cheng, C. Shih, W. Daniel Lewis, T. Koyanagi, T. Hinoki, C. H. Henager Jr and F. Monica, Radiation-tolerant joining technologies for silicon carbide ceramics and composites, *J. Nucl. Mater.*, 2014, **448**(1–3), 497–511.
7 M. A. Khatun, M. H. Mia, S. Ahmad and S. K. Mitro, Crystal stability and the origin of transport properties of new MAX phases Y2AN (A= In, Tl): a theoretical background for experimental study, *Heliyon*, 2025, e42646.
8 T. Cabioch, P. Eklund, M. Vincent, M. Jaouen and M. W. Barsoum, Tailoring of the thermal expansion of Cr2 (Alx, Ge1−x) C phases, *J. Eur. Ceram. Soc.*, 2013, **33**(4), 897–904.
9 M. Radovic, M. W. Barsoum, A. Ganguly, T. Zhen, P. Finkel, S. R. Kalidindi and E. Lara-Curzio, On the elastic properties and mechanical damping of Ti3SiC2, Ti3GeC2, Ti3Si0. 5Al0. 5C2 and Ti2AlC in the 300–1573 K temperature range, *Acta Mater.*, 2006, **54**(10), 2757–2767.
10 J. C. Schuster, H. Nowotny and C. Vaccaro, The ternary systems: CrAlC, VAlC, and TiAlC and the behavior of H-phases (M2AlC), *J. Solid State Chem.*, 1980, **32**(2), 213–219.
11 M. W. Barsoum, I. Salama, T. El-Raghy, J. Golczewski, H. J. Seifert, F. Aldinger, W. D. Porter and H. Wang, Thermal and electrical properties of Nb 2 AlC, (Ti, Nb) 2 AlC and Ti 2 AlC, *Metall. Mater. Trans. A*, 2002, **33**, 2775–2779.
12 I. Salama, T. El-Raghy and M. W. Barsoum, Synthesis and mechanical properties of Nb2AlC and (Ti, Nb) 2AlC, *J. Alloys Compd.*, 2002, **347**(1–2), 271–278.
13 S. Gupta and M. W. Barsoum, Synthesis and oxidation of V 2AlC and (Ti0. 5, V 0.5) 2AlC in air, *J. Electrochem. Soc.*, 2004, **151**(2), D24.

14 H. Yang, B. Manoun, R. T. Downs, A. Ganguly and M. W. Barsoum, Crystal chemistry of layered carbide, Ti3 (Si0. 43Ge0. 57) C2, *J. Phys. Chem. Solids*, 2006, **67**(12), 2512–2516.

15 B. Manoun, S. K. Saxena, G. Hug, A. Ganguly, E. N. Hoffman and M. W. Barsoum, Synthesis and compressibility of Ti3 (Al, Sn0. 2) C2 and Ti3Al (C0. 5, N0. 5) 2, *J. Appl. Phys.*, 2007, **101**, 11.

16 M. W. Barsoum and M. Radovic, 'Elastic and mechanical properties of the MAX phases, *Annu. Rev. Mater. Res.*, 2011, **41**(1), 195–227.

17 H. Kim, J. Choi, J. Choi, J. Kwak and J. Kim, Ab initio simulations of M2AX (M= lanthanides, A= Al or Si, X= C or N) phases as bond coats for thermal barrier coatings, *Scr. Mater.*, 2025, **258**, 116520.

18 O. S. Rijal, H. Krishna Neupane, D. Oli, R. Kiran Neupane, P. Shrestha, S. Sharma, L. P. Joshi and P. Rajendra, A first-principles investigation of the structural, mechanical, dynamic, electronic, magnetic, and optical properties of Ti2AC (A= Cd, S) MAX phase compounds, *J. Phys. D: Appl. Phys.*, 2025, **58**(12), 125102.

19 B. U. Haq, Se-H. Kim, R. Ahmed, A. Rasool Chaudhry, M. Shabbir and A. Laref, Physical properties of W2GaX (X= C, N, and F) based novel MAX phases; potential materials for applications in advanced electronic and optical devices, *Comput. Theor. Chem.*, 2024, **1231**, 114427.

20 M. N. Amin, A. A. Faysal, A. Azzouz-Rached, F. I. Chowdhury, J. Uddin, J. Uddin, J. Islam, A. R. Piyal, A. K. Chowdhury and A. K. M. Rahman, DFT insights into the structural, mechanical, electronic, optical, and thermal properties of Cr2AC (A= Si, Al, Ga, Ge, and P) MAX phases carbides, *AIP Adv.*, 2024, **14**(12), 125302.

21 W. Tan, Y. Tian, Y. Zhou, X. Wei, L. Zhang, X. Tao and Y. Ouyang, Trends in mechanical, anisotropic, electronic, and thermal properties of MAX phases: a DFT study on M2SX phases, *Mater. Today Commun.*, 2023, **35**, 105759.

22 M. A. Ali and W. Q. Muhammad, DFT insights into the new Hf-based chalcogenide MAX phase Hf2SeC, *Vacuum*, 2022, **201**, 111072.

23 M. M. Uddin, MdA. Ali, MdM. Hossain, S. H. Naqib and A. K. M. A. Islam, Comparative study of predicted MAX phase Hf 2 AlN with recently synthesized Hf 2 AlC: a first principle calculations, *Indian J. Phys.*, 2022, 1–13.

24 W. Kohn and J. S. Lu, Self-consistent equations including exchange and correlation effects, *Phys. Rev.*, 1965, **140**(4A), A1133.

25 S. J. Clark, M. D. Segall, C. J. Pickard, P. J. Hasnip, M. I. J. Probert, K. Refson and M. C. Payne, First principles methods using CASTEP, *Z. Kristallogr. Cryst. Mater.*, 2005, **220**(5–6), 567–570.

26 J. P. Perdew, K. Burke and M. Ernzerhof, Generalized gradient approximation made simple, *Phys. Rev. Lett.*, 1996, 77(18), 3865.

27 H. J. Monkhorst and J. D. Pack, Special points for Brillouin-zone integrations, *Phys. Rev. B*, 1976, **13**(12), 5188.

28 D. Vanderbilt, Soft self-consistent pseudopotentials in a generalized eigenvalue formalism, *Phys. Rev. B:Condens. Matter Mater. Phys.*, 1990, **41**(11), 7892.

29 T. H. Fischer and A. Jan, General methods for geometry and wave function optimization, *J. Phys. Chem.*, 1992, **96**(24), 9768–9774.

30 C. M. Brown, W. Dreyer and W. H. Müller, The convergence of a DFT-algorithm for solution of stress-strain problems in composite mechanics, *J. Eng. Mater. Technol.*, 2003, **125**(1), 27–37.

31 K. Parlinski, Z. Q. Li and Y. Kawazoe, First-principles determination of the soft mode in cubic ZrO2, *Phys. Rev. Lett.*, 1997, **78**(21), 4063.

32 K. Momma and F. Izumi, VESTA 3 for three-dimensional visualization of crystal, volumetric and morphology data, *Appl. Crystallogr.*, 2011, **44**(6), 1272–1276.

33 A. Bouhemadou, Structural, Electronic and Elastic Properties of Ti 2 TlC, Zr 2 TlC and Hf 2 TlC, *Cent. Eur. J. Phys.*, 2009, **7**, 753–761.

34 K. Akter, F. Parvin, M. A. Hadi and A. K. M. A. Islam, Insights into the predicted Hf2SN in comparison with the synthesized MAX phase Hf2SC: A comprehensive study, *Comput. Condens. Matter*, 2020, **24**, e00485.

35 A. Roumili, Y. Medkour and D. Maouch, Elastic and Electronic Properties of Hf 2 SnC and Hf 2 SnN, *Int. J. Mod. Phys. B*, 2009, **23**(26), 5155–5161.

36 T. Lapauw, B. Tunca, T. Cabioc'h, J. Lu, P. O. Å. Persson, K. Lambrinou and J. Vleugels, Synthesis of MAX phases in the Hf–Al–C system, *Inorg. Chem.*, 2016, **55**(21), 10922–10927.

37 Q. Zhang, Y. Zhou, X. San, W. Li, Y. Bao, Q. Feng, S. Grasso and C. Hu, Zr2SeB and Hf2SeB: Two new MAB phase compounds with the Cr2AlC-type MAX phase (211 phase) crystal structures, *J. Adv. Ceram.*, 2022, **11**(11), 1764–1776.

38 M. B. Kanoun, S. Goumri-Said and M. Jaouen, Steric effect on the M site of nanolaminate compoundsM2SnC (M= Ti, Zr, Hf and Nb), *J. Phys.:Condens. Matter*, 2009, **21**(4), 045404.

39 M. H. Mia and A. K. Mst, Dynamic tuning of optoelectronic and mechanical properties in TlMCl3 (M= Ge, Sn) under pressure-induced phase transition, *Heliyon*, 2025, e42603.

40 A. B. Alruqi, Engineering the Mechanics and Thermodynamics of Ti3AlC2, Hf3AlC2, Hf3GaC2,(ZrHf) 3AlC2, and (ZrHf) 4AlN3 MAX Phases via the Ab Initio Method, *Crystals*, 2025, **15**(1), 87.

41 M. Dahlqvist, B. Alling and J. Rosén, Stability trends of MAX phases from first principles, *Phys. Rev. B:Condens. Matter Mater. Phys.*, 2010, **81**(22), 220102.

42 L. Sun, L. Miao and Y. Cao, The physical properties of new MAX phase Zr3XC2 (X= Cd, Sb): A DFT investigation, *J. Mater. Sci.*, 2025, 1–19.

43 S. Kirklin, J. E. Saal, B. Meredig, A. Thompson, J. W. Doak, M. Aykol, S. Rühl and C. Wolverton, The Open Quantum Materials Database (OQMD): assessing the accuracy of DFT formation energies, *npj Comput. Mater.*, 2015, **1**(1), 1–15.

44 N. Goossens, B. Tunca, K. Lambrinou and J. Vleugels, Topotactic transformations in Hf-Al-C MAX phase compounds: Synthesis and characterization of

nanolaminated Hf2AlC, Hf3AlC2 and Hf5Al2C3, *Open Ceram.*, 2024, **18**, 100584.
45 L. Chen, Y. Li, K. Chen, X. Bai, M. Li, S. Du, Z. Chai and Q. Huang, Synthesis and characterization of medium-/high-entropy M2SnC (M= Ti/V/Nb/Zr/Hf) MAX phases, *Small Struct.*, 2023, **4**(1), 2200161.
46 Q. Zhang, B. Wen, L. Jia, Y. Zhou, X. San, Y. Bao, L. Chu, Q. Feng, S. Grasso and C. Hu, Synthesis of new lead-containing MAX phases of Zr3PbC2 and Hf3PbC2, *J. Am. Ceram. Soc.*, 2023, **106**(11), 6390–6397.
47 F. Mouhat and F.-X. Coudert, Necessary and sufficient elastic stability conditions in various crystal systems, *Phys. Rev. B:Condens. Matter Mater. Phys.*, 2014, **90**(22), 224104.
48 M. I. Naher and S. H. Naqib, An ab-initio study on structural, elastic, electronic, bonding, thermal, and optical properties of topological Weyl semimetal Ta X (X= P, As), *Sci. Rep.*, 2021, **11**(1), 5592.
49 M. H. Mia, F. Parvin, A. K. M. A. Islam and M. A. Khatun, Ternary chalcogenides NbIn X 2 (X= S, Se): A comprehensive investigation of mechanical, electronic, vibrational, optical and thermophysical properties, *Int. J. Mod. Phys. B*, 2025, **39**(14), 2550118.
50 R. Hill, The elastic behaviour of a crystalline aggregate, *Proc. Phys. Soc., London, Sect. A*, 1952, **65**(5), 349.
51 Y. W. Bao, X. H. Wang, H. B. Zhang and Y. C. Zhou, Thermal shock behavior of Ti3AlC2 from between 200 °C and 1300 °C, *J. Eur. Ceram. Soc.*, 2005, **25**(14), 3367–3374.
52 M. A. Khatun, M. H. Mia, M. A. Hossain, F. Parvin and A. K. M. A. Islam, Optical and thermoelectric properties of layer structured Ba2XS4 (X= Zr, Hf) for energy harvesting applications, *J. Phys. Chem. Solids*, 2025, **196**, 112381.
53 P. H. Mott, J. R. Dorgan and C. M. Roland, The bulk modulus and Poisson's ratio of "incompressible" materials, *J. Sound Vib.*, 2008, **312**(4–5), 572–575.
54 X.-Q. Chen, H. Niu, D. Li and Y. Li, Modeling hardness of polycrystalline materials and bulk metallic glasses, *Intermetallics*, 2011, **19**(9), 1275–1281.
55 N. Miao, S. Baisheng, J. Zhou and Z. Sun, Theoretical investigation on the transition-metal borides with Ta3B4-type structure: A class of hard and refractory materials, *Comput. Mater. Sci.*, 2011, **50**(4), 1559–1566.
56 Md A. Rahman, M. Asma Khatun, Md H. Mia, M. Zugrufa and I. Ahmad, First-Principles Calculations to Investigate the Structural, Mechanical, Electronic, Optical and Thermal Properties of Disilicides Materials UT2Si2 (T= Ru, Rh, and Pd), *Phys. Status Solidi B*, 2025, **262**(1), 2400230.
57 P. Ravindran, L. Fast, P. A. Korzhavyi, B. Johansson, J. Wills and E. Os, Density functional theory for calculation of elastic properties of orthorhombic crystals: Application to TiSi 2, *J. Appl. Phys.*, 1998, **84**(9), 4891–4904.
58 C. M. Kube and D. J. Maarten, Elastic constants of polycrystals with generally anisotropic crystals, *J. Appl. Phys.*, 2016, **120**(16), 165105.
59 S. I. Ranganathan and M. Ostoja-Starzewski, Universal elastic anisotropy index, *Phys. Rev. Lett.*, 2008, **101**(5), 055504.
60 M. H. Mia, M. A. Khatun and M. Rahman, Ti2PTe2 chalcogenide: A comprehensive DFT study on physical properties, *Next Mater.*, 2025, **7**, 100434.
61 E. Schreiber, O. L. Anderson, N. Soga, and J. F. Bell, '*Elastic Constants and Their Measurement*', 1975, pp. 747–748.
62 O. L. Anderson, A simplified method for calculating the Debye temperature from elastic constants, *J. Phys. Chem. Solid.*, 1963, **24**(7), 909–917.
63 M. E. Fine, L. D. Brown and H. L. Marcus, Elastic constants versus melting temperature in metals, *Scripta Metall.*, 1984, **18**(9), 951–956.
64 V. N. Belomestnykh and E. P. Tesleva, Interrelation between Anharmonicity and Lateral Strain in Quasi-Isotropic Polycrystalline Solids, *Tech. Phys.*, 2004, **49**(8), 1098.
65 C. Dhakal, S. Aryal, R. Sakidja and W.-Y. Ching, Approximate lattice thermal conductivity of MAX phases at high temperature, *J. Eur. Ceram. Soc.*, 2015, **35**(12), 3203–3212.
66 C. L. Julian, Theory of heat conduction in rare-gas crystals, *Phys. Rev.*, 1965, **137**(1A), A128.
67 D. R. Clarke, Materials selection guidelines for low thermal conductivity thermal barrier coatings, *Surf. Coating. Technol.*, 2003, **163**, 67–74.
68 M. W. Qureshi, X. Ma, G. Tang and P. Ramesh, Structural stability, electronic, mechanical, phonon, and thermodynamic properties of the M2GaC (M= Zr, Hf) max phase: an AB initio calculation, *Materials*, 2020, **13**(22), 5148.
69 M. A. Hadi, N. Kelaidis, S. H. Naqib, A. K. M. A. Islam, A. Chroneos and R. V. Vovk, Insights into the physical properties of a new 211 MAX phase Nb2CuC, *J. Phys. Chem. Solids*, 2021, **149**, 109759.
70 Y. Mo, R. Paul and W. Y. Ching, Electronic structure and optical conductivities of 20 MAX-phase compounds, *Phys. Rev. B:Condens. Matter Mater. Phys.*, 2012, **86**(16), 165122.
71 M. D. Segall, R. Shah, C. J. Pickard and M. C. Payne, Population analysis of plane-wave electronic structure calculations of bulk materials, *Phys. Rev. B*, 1996, **54**(23), 16317.
72 F. L. Hirshfeld, Bonded-atom fragments for describing molecular charge densities, *Theor. Chim. Acta*, 1977, **44**, 129–138.
73 M. Tarekuzzaman, N. Shahadath, M. Montasir, O. Alsalmi, M. H. Mia, H. Al-Dmour, M. Rasheduzzaman and M. Z. Hasan, DFT analysis of the physical properties of direct band gap semiconducting double perovskites A 2 BIrCl 6 (A= Cs, Rb; B= Na, K) for solar cells and optoelectronic applications, *RSC Adv.*, 2025, **15**(17), 13643–13661.
74 O. Das, J. K. Rony, P. Kumar Karmaker, M. A. Khatun, Md Murshidul Islam, M. H. Mia, M. Saiduzzaman and M. Islam, Tailoring the physical properties of InSnX3 (X= F, cl) perovskites via pressure: A path toward sustainable optoelectronics, *Chem. Phys.*, 2025, 112635.
75 S. Li, R. Ahuja, M. W. Barsoum, P. Jena and B. Johansson, Optical properties of Ti3SiC2 and Ti4AlN3, *Appl. Phys. Lett.*, 2008, **92**, 22.
76 M. A. Ali, M. M. Hossain, M. M. Uddin, A. K. M. A. Islam and S. H. Naqib, Understanding the improvement of thermo-

mechanical and optical properties of 212 MAX phase borides Zr2AB2 (A= In, Tl), *J. Mater. Res. Technol.*, 2021, **15**, 2227–2241.

77 M. R. Khatun, M. A. Ali, F. Parvin and A. K. M. A. Islam, Elastic, thermodynamic and optical behavior of V2AC (A= Al, Ga) MAX phases, *Results Phys.*, 2017, **7**, 3634–3639.

78 M. W. Qureshi, M. A. Ali and X. Ma, Screen the thermomechanical and optical properties of the new ductile 314 MAX phase boride Zr3CdB4: A DFT insight, *J. Alloys Compd.*, 2021, **877**, 160248.

79 M. A. Hadi, Y. Panayiotatos and A. Chroneos, Structural and optical properties of the recently synthesized (Zr3−x Ti x) AlC2 MAX phases, *J. Mater. Sci.: Mater. Electron.*, 2017, **28**(4), 3386–3393.

80 A. Chowdhury, M. A. Ali, M. M. Hossain, M. M. Uddin, S. H. Naqib and A. K. M. A. Islam, Predicted MAX phase Sc2InC: dynamical stability, vibrational and optical properties, *Phys. Status Solidi B*, 2018, **255**(3), 1700235.